

# 1 **Mid-Holocene European climate revisited: new high-resolution regional climate** 2 **model simulations using pollen-based land-cover**

3 Gustav Strandberg<sup>1,2,\*</sup>, Johan Lindström<sup>3</sup>, Anneli Poska<sup>4,8</sup>, Qiong Zhang<sup>2,5</sup>, Ralph Fyfe<sup>6</sup>, Esther  
4 Githumbi<sup>7,8</sup>, Erik Kjellström<sup>1,2</sup>, Florenze Mazier<sup>9</sup>, Anne-Birgitte Nielsen<sup>10</sup>, Shinya Sugita<sup>11</sup>, Anna-  
5 Kari Trondman<sup>7,12</sup>, Jessie Woodbridge<sup>6</sup>, Marie-José Gaillard<sup>7</sup>

6  
7 <sup>1</sup> Rossby Centre, Swedish Meteorological and Hydrological Institute, SMHI, Norrköping, SE-602  
8 19, Sweden

9 <sup>2</sup> Bolin Centre for Climate Research, Stockholm University, Stockholm, SE-106 91, Sweden

10 <sup>3</sup> Centre for Mathematical Sciences, Lund University, SE-221 00 Lund, Sweden

11 <sup>4</sup> Department of Geology, Tallinn University of Technology, 19086 Tallinn, Estonia

12 <sup>5</sup> Department of Physical Geography, Stockholm University, Stockholm, SE-106 91, Sweden

13 <sup>6</sup> School of Geography, Earth and Environmental Sciences, University of Plymouth, Plymouth PL4  
14 8AA, UK.

15 <sup>7</sup> Department of Biology and Environmental Science, Linnaeus University, SE-39231 Kalmar,  
16 Sweden

17 <sup>8</sup> Department of Physical Geography and Ecosystem Science, Lund University, SE-221 00, Sweden

18 <sup>9</sup> Department of Environmental Geography, UMR-CNRS 5602, Toulouse Jean Jaurès University,  
19 Toulouse, C229, France.

20 <sup>10</sup> Department of Geology, Lund University, SE-221 00, Sweden

21 <sup>11</sup> Institute of Ecology, Tallinn University, Tallinn, Estonia

22 <sup>12</sup> Division of Educational Affairs, Swedish University of Agricultural Sciences, Lomma, SE-234  
23 22, Sweden

24  
25 \* Corresponding author. E-mail adress: [gustav.strandberg@smhi.se](mailto:gustav.strandberg@smhi.se) (G. Strandberg)

26  
27 **Keywords:** paleoclimate, global climate model, dynamical vegetation model, vegetation  
28 reconstruction, spatial statistical models, land-use and land-cover change, REVEALS, LPJ-GUESS,  
29 EC-Earth, RCA4, HCLIM

## 30 **Highlights:**

- 31 • First simulation of paleoclimate using more than one regional climate model.
- 32
- 33 • Estimates of Mid-Holocene vegetation constructed both by dynamical vegetation model and  
34 pollen records and statistical methods.
- 35 • This approach enables us to study differences between modeled and reconstructed  
36 vegetation, and the response to land-cover changes in regional climate models.
- 37 • Results indicate that the anthropogenic land-cover changes are large enough to have a  
38 significant impact on European climate already at Mid-Holocene.

39  
40 **Competing interest statement:** The authors declare that they have no known competing financial  
41 interests or personal relationships that could have appeared to influence the work reported in this  
42 paper.

43  
44 **CRedit author statement:** **Gustav Strandberg:** Conceptualisation, Methodology, Formal  
45 analysis, Investigation, Writing – Original Draft, Visualisation; **Johan Lindström:**  
46 Conceptualisation, Methodology, Formal analysis, Investigation, Writing – Review & Editing;  
47 **Anneli Poska:** Conceptualisation, Methodology, Formal analysis, Investigation, Writing – Review  
48 & Editing, Visualisation; **Qiong Zhang:** Conceptualisation, Methodology, Investigation, Writing –  
49 Review & Editing; **Ralph Fyfe:** Methodology, Formal analysis, Investigation, Writing – Review &

50 Editing; **Esther Githumbi**: Conceptualisation, Methodology, Formal analysis, Investigation,  
51 Writing – Review & Editing; **Erik Kjellström**: Conceptualisation, Writing – Review & Editing ;  
52 **Florenze Mazier**: Methodology, Investigation, Writing – Review & Editing; **Anne-Birgitte**  
53 **Nielsen**: Conceptualisation, Writing – Review & Editing; **Shinya Sugita**: Methodology, Writing –  
54 Review & Editing; **Anna-Kari Trondman**: Methodology, Investigation; **Jessie Woodbridge**:  
55 Methodology, Investigation, Writing – Review & Editing; **Marie-José Gaillard**:  
56 Conceptualisation, Writing – Review & Editing, Project administration, Funding acquisition.  
57

## 58 **Abstract**

59 Land-cover changes have a clear impact on local climates via biophysical effects. European land  
60 cover has been affected by human activities for at least 6000 years, but possibly longer. It is thus  
61 highly probable that humans altered climate before the industrial revolution (AD 1750 to 1850). In  
62 this study, climate and vegetation 6000 years (6 ka) ago is investigated using one global climate  
63 model, two regional climate models, one dynamical vegetation model, pollen-based reconstruction  
64 of past vegetation cover using a model of the pollen-vegetation relationship and a statistical model  
65 for spatial interpolation of the reconstructed land cover. This approach enables us to study 6 ka  
66 climate with potential natural and reconstructed land cover, and to determine how differences in  
67 land cover impact upon simulated climate. The use of two regional climate models enables us to  
68 discuss the robustness of the results. This is the first experiment with two regional climate models  
69 of simulated palaeo-climate based on regional climate models.

70 Different estimates of 6 ka vegetation are constructed: simulated potential vegetation and  
71 reconstructed vegetation. Potential vegetation is the natural climate-induced vegetation as simulated  
72 by a dynamical vegetation model driven by climate conditions from a climate model. Bayesian  
73 spatial model interpolated point estimates of pollen-based plant abundances combined with  
74 estimates of climate-induced potential un-vegetated land cover were used for reconstructed  
75 vegetation. The simulated potential vegetation is heavily dominated by forests: evergreen  
76 coniferous forests dominate in northern and eastern Europe, while deciduous broadleaved forests  
77 dominate central and western Europe. In contrast, the reconstructed vegetation cover has a large  
78 component of open land in most of Europe.

79 The simulated 6 ka climate using reconstructed vegetation was 0-5 °C warmer than the pre-  
80 industrial (PI) climate, depending on season and region. The largest differences are seen in north-  
81 eastern Europe in winter with about 4-6°C, and the smallest differences (close to zero) in  
82 southwestern Europe in winter. The simulated 6 ka climate had 10-20 % more precipitation than PI  
83 climate in northern Europe and 10-20 % less precipitation in southern Europe in summer. The  
84 results are in reasonable agreement with proxy-based climate reconstructions and previous similar  
85 climate modelling studies. As expected, the global model and regional models indicate relatively  
86 similar climates albeit with regional differences indicating that, models response to land-cover  
87 changes differently.

88 The results indicate that the anthropogenic land-cover changes, as given by the reconstructed  
89 vegetation, in this study are large enough to have a significant impact on climate. It is likely that  
90 anthropogenic impact on European climate via land-use change was already taking place at 6 ka.  
91 Our results suggest that anthropogenic land-cover changes at 6 ka lead to around 0.5 °C warmer in  
92 southern Europe in summer due to biogeophysical forcing.

93

## 94 **1 Introduction**

95 Land-use and land-cover change (LULCC) as a means of climate-change mitigation has received  
96 an increasing interest in recent years (e.g. Smith et al., 2016a; Williamson, 2016; Griscom et al.,  
97 2017). Emissions scenarios compliant with the goal of the Paris Agreement to limit global warming  
98 to “well below 2 degrees” (UNFCCC, 2010; UNFCCC, 2015) are partly reliant upon different ways  
99 to achieve carbon uptake, capture and sequestration (IPCC, 2018). Meeting these targets implies  
100 that LULCC will need to change drastically at the global scale over the coming decades. In theory,  
101 afforestation as mitigation measure could limit global warming because increased biomass would  
102 decrease the amount of carbon dioxide (CO<sub>2</sub>) in the atmosphere via biogeochemical processes,  
103 primarily carbon fixation by plants via photosynthesis. Further, bioenergy with carbon capture and  
104 storage (BECCs) has become to be considered as one of the most realistic and cost-effective

105 technologies for negative emissions as it combines the use of biomass with geological storage of  
106 CO<sub>2</sub>. However, changes in land-cover also have biogeophysical effects affecting the albedo, surface  
107 roughness and heat fluxes (e.g. plant evapotranspiration), which in turn will influence regional  
108 climate and may limit the positive effect of a wide-spread application of such mitigation measures  
109 (e.g. Smith et al., 2016a). The biogeophysical effects have been less studied than the  
110 biogeochemical ones. However, several studies have shown that regional climatic responses to  
111 LULCC can differ depending on the season and the geographical location (e.g. Jia et al., 2019;  
112 Strandberg & Kjellström, 2019). Thus, the overall positive global effects of land cover-based  
113 mitigation strategies may have negative regional effects.

114 Henceforth, we use the term LULCC primarily to describe deforestation by humans, i.e.  
115 replacement of tree vegetation by low vegetation (herbs and low shrubs), although past land-use  
116 changes have had other consequences on land cover, such as transformation of grazing and  
117 cultivated land into woodland due to shifting cultivation or land abandonment. LULCC is thus  
118 synonym of “anthropogenic land-cover change” (ALCC) (e.g. Kaplan et al., 2009), a term also  
119 commonly used in the literature. The identification of the most suitable climate-change mitigation  
120 strategies still requires a better understanding of the biogeophysical effects of LULCC on climate,  
121 and a better estimate of the net effects (biogeo-physical and – chemical). This can be achieved with  
122 idealized climate model simulations, e.g. evaluating the effect of complete afforestation or  
123 deforestation of a large area of the globe such as a continent (e.g. Boysen et al., 2020; Davin et al.,  
124 2020). It can also be studied with palaeoclimate model simulations using reconstructions of past  
125 LULCC over long time periods, and either Global Climate Models (GCMs) (He et al., 2014; Smith  
126 et al., 2016b; Gilgen et al., 2019) or regional climate models (RCMs) (Strandberg et al., 2014;  
127 Russo and Cubash, 2016; Velasquez et al., 2021). Such studies have the advantage to investigate the  
128 effects of realistic LULCC on past climate, and climate-model simulations can be evaluated with  
129 palaeoclimate proxies. However, such studies are few; moreover, it has also been argued that the  
130 study of LULCC as a climate forcing requires the use of high-resolution RCMs to better account for

131 the biogeophysical forcing of LULCC that operates at a regional scale rather than at a global scale  
132 (e.g. Gaillard et al., 2010; Strandberg et al., 2014). The higher density of the horizontal grid spacing  
133 in RCMs (usually 10-50 km) than in GCMs (usually 100 - 200 km) (e.g. Rummukainen, 2016) is  
134 also an advantage in palaeoclimate modelling if the model output is to be compared with proxy data  
135 that generally represent local scale climate (Ludwig et al., 2018; Ludwig et al., 2019; Giorgi, 2019).  
136 Only two such studies using RCMs exist for Europe (Strandberg et al., 2014; Russo and Cubash,  
137 2016). These studies were first attempts at evaluating the potential of RCMs to study climate  
138 conditions during the Holocene at the European scale. They provided new insights on temperature  
139 difference (Strandberg et al., 2014) and temperature changes (Russo & Cubash, 2016; Russo et al.,  
140 2021) between 6000 years BP (henceforth 6 ka; Mid Holocene conditions) and 1750 CE (200 years  
141 BP, henceforth 0.2 ka). Strandberg et al. (2014) also investigated the effect of LULCC at 6 ka and  
142 0.2 ka. Both studies demonstrated the need for more RCM studies of Holocene climate to better  
143 understand past climate change and climate forcings at a regional scale, and in particular further  
144 elucidate the regional effect of LULCC in Europe.

145 In this study, we revisit the climate in Europe at 6 ka (representing Mid Holocene and the  
146 “Neolithic Revolution”) and 1850, a pre-industrial time slice commonly used to represent a base  
147 line for the most recent climate that is little influenced by human activities (henceforth PI). The  
148 objective is to investigate the sensitivity of regional climate models (RCMs) (in terms of simulated  
149 climate) to the first substantial LULCC in Europe related to the “Neolithic revolution”, i.e. the  
150 introduction of crop cultivation and cattle grazing (e.g. Bocquet-Appel, 2011), in comparison with  
151 no LULCC (i.e. climate-induced, natural vegetation, also termed “potential vegetation”). The 6 ka  
152 climate (with and without LULCC) is then compared with PI climate; a recent period that is still not  
153 that affected by anthropogenic greenhouse gas emissions . The major differences between this new  
154 study and that of Strandberg et al. (2014) are (a) the use of two RCM models instead of one and (b)  
155 pollen-based LULCC reconstructions as land-use forcing, rather than LULCC scenarios such as the  
156 commonly used KK10 (Kaplan et al., 2009) or HYDE (Klein Goldewijk et al., 2017) scenarios. The

157 latter are largely based on population growth models and hypotheses. It is the first time that the use  
158 of more realistic LULCC reconstructions (based on empirical pollen data) is tested at the scale of  
159 Europe. We use the latest pollen-based REVEALS land-cover reconstruction for Europe (Githumbi  
160 et al., 2021), i.e. an extension of the reconstruction by Trondman et al. (2015) both in terms of  
161 number of pollen records used and spatial coverage. It is a gridded reconstruction with a spatial  
162 scale of one degree. REVEALS is a model of the pollen-vegetation relationship integrating models  
163 of dispersion of small particles in the air and their deposition (Sugita 2007). Such pollen-based  
164 REVEALS datasets of past land cover have not been used in climate modelling thus far, although  
165 these reconstructions now exist for over most of the northern hemisphere (e.g. Dawson et al., 2018).  
166 Because of the gaps in the spatial distribution of pollen records, the gridded REVEALS  
167 reconstruction is interpolated into a continuous gridded land-cover dataset for its use in RCM  
168 simulations. This is achieved with spatial statistical models (e.g. Pirzamanbein et al., 2014; 2020).  
169 Potential vegetation, i.e. land cover without LULCC, is simulated by a dynamic vegetation model  
170 (DVM).

171 Comparison between 6 ka and PI climates at the regional scale has also an interest within the  
172 ‘Holocene temperature conundrum’ (HTC) debate (e.g. Liu et al., 2014; Bader et al., 2020). HTC  
173 refers to the disagreement between the Holocene expected global warming due to increasing  
174 greenhouse gases and retreating ice sheets as simulated by global climate models, and the Holocene  
175 cooling shown by the first global palaeoecological reconstruction of Holocene climate (Marcott et  
176 al., 2013). Among the explanations of the HTC, both deficiencies in climate models and in the  
177 analysis of climate-model outputs, as well as biases in the palaeoecological global reconstruction  
178 have been proposed (e.g. Liu et al., 2014). Both HTC and regional data-model inconsistencies have  
179 also been hypothesised to be partly a consequence of not adequately accounting for LULCC from c.  
180 6 ka in Europe (e.g. Kaplan et al., 2010; Ruddiman et al., 2015; Stocker et al. 2017; Harrison et al.,  
181 2018, 2020). In this paper, we also revisit this question in the light of our results.

182

## 183 **2 Models and data**

### 184 **2.1 Model chain**

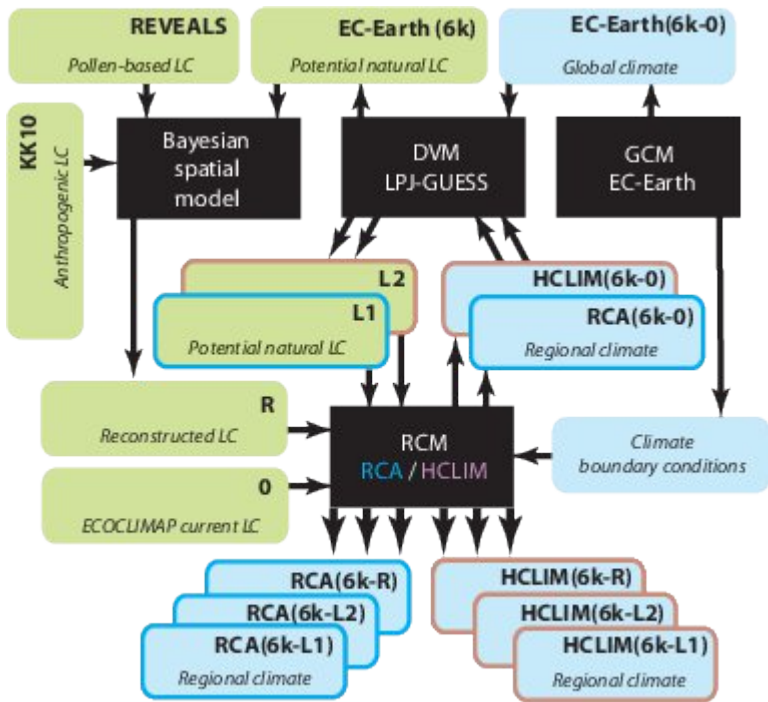
185 This study builds upon a chain of model simulations (see detailed model descriptions below).

186 Within the first step, 6 ka and pre-industrial (1850 CE, hereafter PI) climate conditions are  
187 simulated by the GCM EC-Earth using present day vegetation (Fig. 1 and Table 1). These climate  
188 conditions are then used to force the RCMs RCA4 and HCLIM over the European domain; thus,  
189 simulating the climate at the same periods as the GCM, but at higher horizontal resolution and with  
190 their own physical parameterisations. For each RCM, the model output includes a high-resolution  
191 climate simulation for 6 ka and PI respectively (6k-0 and PI in Table 1). The two representations of  
192 6 ka climate, as simulated by the RCMs, are used to force the DVM LPJ-GUESS to estimate a  
193 potential vegetation cover consistent with each simulated climate. Under 6 ka climate condition,  
194 two simulated potential vegetation cover reconstructions are estimated, one based on EC-  
195 Earth+RCA4+LPJ-GUESS (L1 in Table 1) driven by climate simulated by RCA4 and one based on  
196 EC-Earth+HCLIM+LPJ-GUESS (L2 in Fig. 1 and Table 1) driven by climate simulated by HCLIM.  
197 In this context, ‘potential’ refers to vegetation that is allowed to grow freely without human  
198 intervention, i.e. it is the natural climate-induced vegetation as simulated by the DVM. These two  
199 vegetation covers are then fed back to both RCA4 and HCLIM to simulate 6 ka climate with  
200 vegetation cover consistent with simulated mid-Holocene climate (6k-L1 when land cover L1 is  
201 used and 6k-L2 when L2 is used). PI vegetation is assumed to be the same as the present vegetation,  
202 and is not simulated by LPJ-GUESS.

203

204

205



206 Legend: → flow direction ■ model □ climate / ■ landcover (LC) data □ RCA / □ HCLIM

207 **Figure 1** Description of the model chain for 6 ka. All RCM simulations read boundary conditions  
 208 from EC-Earth. A first set of simulations are made with current land cover (0), these climate  
 209 scenarios are used in LPJ-GUESS to provide the 6 ka potential natural land cover (L1, L2)  
 210 subsequently used in the RCMs. A Bayesian spatial model is used to reconstruct 6 ka land cover (R)  
 211 that is also used in the RCMs.

212

213 In parallel, the 6 ka vegetation is reconstructed at a 1° spatial scale using multiple pollen records  
 214 and the REVEALS model (Sugita, 2007; Githumbi et al., 2021). Proxy-based vegetation cover is  
 215 not available for all 1° grid cells due to the irregular distribution of pollen records. Therefore,  
 216 pollen-based vegetation cover is interpolated over the entire grid covering Europe using spatial  
 217 statistics (Pirzamanbein et al., 2018) and additional co-variates including simulated vegetation from  
 218 LPJ-GUESS (driven by the EC-Earth simulation) and the KK10 anthropogenic land-cover scenario  
 219 for 6 ka (Kaplan et al, 2009). This reconstruction (6k-R in Fig. 1 and Table 1) represents the  
 220 “actual” 6 ka vegetation, i.e. a combination of climate-induced potential vegetation and human-  
 221 induced vegetation.



222 The benefit of this approach compared to coupled simulations is that it is possible to carry out  
 223 sensitivity tests using different vegetation cover estimates in otherwise similar simulations. This  
 224 allows us to study the effect of vegetation on climate, and how this effect is simulated in different  
 225 RCMs. It also allows a multi-model estimate of 6 ka vegetation and climate to be produced.

226  
 227 **Table 1.** The combination of models and land cover (LC) used in each simulation. The DVM is  
 228 driven by climate conditions from RCA4(6k-0) and HCLIM(6k-0) which yields the new LCs L1  
 229 and L2 respectively; these are then used in subsequent climate simulations.

Simulation	Time	GCM	RCM	LC	DVM	New LC
RCA(PI)	PI	EC-Earth3-LR	RCA4	Current veg.		
HCLIM(PI)	PI	EC-Earth3-LR	HCLIM	Current veg.		
RCA(6k-0)	6 ka	EC-Earth3-LR	RCA4	Current veg.	LPJ-GUESS	→L1
HCLIM(6k-0)	6 ka	EC-Earth3-LR	HCLIM	Current veg.	LPJ-GUESS	→L2
RCA(6k-L1)	6 ka	EC-Earth3-LR	RCA4	L1		
RCA(6k-L2)	6 ka	EC-Earth3-LR	RCA4	L2		
HCLIM(6k-L1)	6 ka	EC-Earth3-LR	HCLIM	L1		
HCLIM(6k-L2)	6 ka	EC-Earth3-LR	HCLIM	L2		
RCA(6k-R)	6 ka	EC-Earth3-LR	RCA4	Reconstruction		
HCLIM(6k-R)	6 ka	EC-Earth3-LR	HCLIM	Reconstruction		

230

231

232 **2.2 EC-Earth3-LR**

233 The lateral boundary conditions for the RCMs are taken from simulations with the fully coupled  
234 general circulation model EC-Earth version 3.1 (Hazeleger et al., 2010) with active atmosphere  
235 (IFS), land (H-TESSSEL), ocean (NEMO3.6), and sea-ice (LIM3) components. The atmospheric  
236 component has T159 horizontal spectral resolution (approximately  $1.125^\circ \times 1.125^\circ$ ) with 62 vertical  
237 levels. The Ocean model NEMO (Madec, 2008) has a horizontal resolution of approximately  $1^\circ \times$   
238  $1^\circ$  and 46 vertical levels. The ocean surface part is coupled with the sea-ice model LIM3  
239 (Vancoppenolle et al., 2009). The atmospheric (IFS) and oceanic models (NEMO-LIM) are coupled  
240 through the coupler OASIS3 (Valcke, 2013) every three hours. In past years, the EC-Earth3-LR has  
241 been used to study the mid-Holocene climate change e.g. the climate response to a greening of  
242 Sahara (Muschitiello et al., 2015, Pausata et al., 2016, Lu et al., 2018).

243

244 The PI (1850 CE) and 6 ka simulations are performed following the PMIP4 protocol (Otto-Bliesner  
245 et al., 2017). For the 6 ka simulation, the changes in climate forcing are orbital parameters and CO<sub>2</sub>  
246 and methane concentration. The orbital forcing is calculated in the model according to Berger  
247 (1978) for PI and 6 ka. The CO<sub>2</sub> concentration is 284.7 ppm<sub>v</sub> for PI and 264.4 ppm<sub>v</sub> for 6 ka, and  
248 methane concentration is 760 ppb<sub>v</sub> for PI and 650 ppb<sub>v</sub> for PI. All other climate forcing factors (i.e.  
249 aerosols) and boundary conditions (i.e. land-sea mask, orography) are the same in PI and 6 ka. The  
250 vegetation cover used in PI and 6k-0 simulations was prescribed based on modern satellite  
251 observations (ECMWF, 2009). The model setup for PI and 6 ka with EC-Earth3-LR is the same as  
252 the PMIP4 simulations as described in Zhang et al. (2021). The 6 ka simulation is run for a 500 year  
253 period, the initial conditions are from a 700-year PI spin-up run. The climate quasi-equilibrium  
254 (defined as a global mean surface temperature trend of less than 0.05 °C per century and a stable  
255 Atlantic meridional overturning circulation (Kageyama et al., 2018)) is reached after 200 years and  
256 we use 6-hourly data as the lateral boundary condition for the RCMs.

257

## 258 **2.3 RCA4 and HCLIM**

259 The use of regional climate models (RCM) adds geographical details and improves the simulation  
260 of climatic processes as the horizontal grid spacing is denser in RCMs (usually 10-50 km) than in  
261 GCMs (usually 100 - 200 km) (e.g. Rummukainen, 2016). The Rossby Centre Atmosphere model  
262 (RCA4, Strandberg et al., 2015; Kjellström et al., 2016) has been widely used for modelling future  
263 climate; mainly over Europe, but also for many other parts of the world (e.g. Dosio et al., 2020,  
264 Rana et al., 2020). RCA3, the predecessor of RCA4, has also been used in studies of palaeoclimate  
265 (MIS 3, Kjellström et al., 2010; LGM, Strandberg et al., 2011; 6 ka, Strandberg et al., 2014; the last  
266 millennium, Schimanke et al., 2012). Here, RCA4 is run with 24 vertical levels and a time step of  
267 20 min, made possible by semi-Lagrangian discretisation (Källén, 1996). Radiation is parameterised  
268 with the Savijärvi HIRLAM radiation scheme (Savijärvi, 1990), turbulence with the CBR turbulent  
269 kinetic energy based scheme (Marquet, 2008), condensation and convection with the Bechtold-KF  
270 scheme (Bechtold et al., 2001). Land surface processes are parameterised with the RCA land-  
271 surface scheme (Samuelsson et al., 2006).

272 The HCLIM38-ALADIN (HCLIM, Belušić et al., 2020) has been used in future climate simulations  
273 for European, African and Arctic domains (Belušić et al., 2020; Lind et al., 2020). HCLIM is run  
274 with 65 vertical levels and a time step of 20 min, made possible by a semi Lagrangian scheme  
275 (Ritchie et al., 1995; Robert et al., 1972; Simmons et al., 1978; Temperton et al., 2001). Convection  
276 is parameterised with KFB (Bechtold et al., 2001; Bazile et al., 2012), micro-physics from Lopez  
277 (2002) and Bouteloup et al. (2005), turbulence with CBR (Cuxart et al., 2000), land surface  
278 processes with SURFEX (Masson et al., 2013) and radiation with RRTM\_LW, SW6 (Mlawer et al.,  
279 1997; Iacono et al., 2008; Fouquart and Bonnel, 1980).

280 Both RCMs are run on a horizontal grid spacing of  $0.44^\circ$  (corresponding to approximately 50 km)  
281 across Europe (the CORDEX EUR-44 domain (Jacob et al., 2014)). Every 6 h, the RCMs read  
282 humidity, temperature, wind and surface pressure from EC-Earth3-LR along the lateral boundaries  
283 of the model domain, and sea surface temperature and sea ice extent within the model domain.

284 Changing orbital forcing is not an option in the current versions of the RCMs used here. The solar

285 constant and amount of greenhouse gases are maintained at pre-industrial levels in all experiments.  
286 The RCMs should nevertheless be able to reproduce 6 ka climate as the climate to a large degree is  
287 governed by the GCM (Kjellström et al., 2018; Vautard et al., 2020; Strandberg & Lind, 2021) even  
288 with different insolation (Kjellström et al., 2010). For PI, a simulation of 30 years is analysed, for 6  
289 ka a 50 year period. We calculate the average of the nominal season's winter (December, January  
290 and February; henceforth DJF) and summer (June, July and August; henceforth JJA).

291

## 292 **2.4 LPJ-GUESS**

293 The dynamic vegetation model (DVM) LPJ-GUESS (Lund-Potsdam-Jena General Ecosystem  
294 Simulator) used in this study is an individual-based ecosystem model optimized for regional studies  
295 (Smith et al., 2001; Sitch et al., 2003; Smith et al., 2014). Model performance in terms of  
296 reproducing vegetation, hydrological and biogeochemical cycles for past applications has been  
297 tested in several studies (Miller et al., 2008; Garreta et al., 2010; Lu et al., 2018). The model has  
298 been repeatedly applied and benchmarked for European conditions (Miller et al., 2008; Hickler et  
299 al., 2012). LPJ-GUESS has been run together with RCA3 for different time periods (Kjellström et  
300 al., 2010; Strandberg et al., 2011; Strandberg et al., 2014).

301 In order to simulate potential natural vegetation cover for Europe at 6 ka, LPJ-GUESS used the  
302 climate input scenarios from the GCM and RCMs described above. LPJ-GUESS reads temperature,  
303 precipitation (amount and number of days) and radiation (in- and outgoing short- and longwave)  
304 from the climate models. The spatial resolution of the simulations was inherited from the climate  
305 inputs. The CO<sub>2</sub> level was set to 265 ppm (Augustin et al 2004), which is almost the same  
306 concentration as the forcing set in EC-Earth3-LR 6 ka simulation. In order to reach a stable  
307 vegetation composition, a spin-up period of 300 years was implemented using the first 10 years of  
308 the simulation in a randomized way. A set of plant functional types (PFTs) based on major  
309 European tree species was applied (Hickler et al., 2012). Vegetation cover fractions were calculated  
310 based on the averaged output of PFT specific leaf area index (LAI) over the last 30 years of the

311 simulation period. The LAI was converted into fractional plant cover (FPC) using a simplified  
 312 version of the Lambert-Beer's law:  $FPC=(1.0-\exp(-0.5*LAI_{PFT}))$  (Monsi & Saeki 1953, Prentice et  
 313 al., 1993). The vegetation input for the RCMs was generated by summing the FPCs of the simulated  
 314 PFTs into three land-cover types: summer-green trees (ST), evergreen trees (ET) and open land  
 315 (OL) (Table 2). The fraction of non-vegetated area was estimated by subtracting summed vegetation  
 316 cover from one. For usage as co-variate in the spatial interpolation model, the vegetation cover  
 317 fractions were proportionally reduced by the anthropogenic land-cover deforestation estimate at 6  
 318 ka derived from the ALCC model KK10 (Kaplan et al., 2011).  
 319

**Table 2** Groups of land-cover types used in this study. Ericaceae\*(MTSE): the pollen productivity used for Ericaceae pollen in the REVEALS reconstruction represents the mean pollen productivity of several species of which *Arbutus unedo*, *Erica arborea*, *E. cinerea* and *E. multiflora* are dominant. The genus *Calluna vulgaris* (heather, LSE) also belongs to the Ericaceae family but its pollen productivity has been estimated separately (Githumbi et al., 2021). Cerealia t.: all cereals except *Secale cereale* (rye) that is easily that is easily separated on the basis of pollen morphology and for which pollen productivity was estimated separately. Abbreviation: t = type. of land-cover types (LCTs) and Plant Functionnal Types (PFTs) used in this study. \*\*The most recent plant taxonomy has merged the family Chenopodiaceae into the family Amaranthaceae, i.e. "new" Amaranthaceae = "former" Amaranthaceae + Chenopodiaceae. Pollen analysts have mostly used the name Chenopodiaceae for this pollen-morphological type, but it includes all species from the two former families, therefore the name Amaranthaceae/Chenopodiaceae.

<b>Land-cover</b>			
<b>types</b>	<b>Plant taxa/Pollen-</b>		
<b>(LCTs)</b>	<b>PFT</b>	<b>PFT definition</b>	<b>morphological types</b>
Evergreen trees and shrubs (ET)	TBE1	Shade-tolerant evergreen trees	<i>Picea abies</i> (Norway spruce)
	TBE2	Shade-tolerant evergreen trees	<i>Abies alba</i> (Silver fir)
	IBE	Shade-intolerant evergreen trees	<i>Pinus sylvestris</i> (Scots

		pine)
		<i>Phillyrea</i> (mock privet)
MTBE	Mediterranean shade-tolerant broadleaved evergreen trees	<i>Pistacia</i> (lentisk, mastic)
		<i>Quercus evergreen t.</i> (evergreen oak species)
TSE	Tall shrub, evergreen	<i>Juniperus communis</i> (common juniper)
MTSE	Mediterranean broadleaved tall shrubs, evergreen	Ericaceae* (heather family) <i>Buxus sempervirens</i> (common box)
IBS	Shade-intolerant summer-green trees	<i>Alnus glutinosa</i> (common alder)
		<i>Betula</i> (birch species)
		<i>Carpinus betulus</i> (common hornbeam)
Summer-green trees and shrubs (ST)		<i>Carpinus orientalis</i> (oriental hornbeam)
	TBS	Shade-tolerant summer-green trees <i>Castanea sativa</i> (sweet chestnut)
		<i>Corylus avellana</i> (common hazel)
		<i>Fagus sylvatica</i> (European beech)
		<i>Fraxinus</i> (ash species)

			<i>Quercus deciduous t.</i> (summer-green oak species)
			<i>Tilia</i> (linden species)
			<i>Ulmus</i> (elm species)
	TSD	Tall shrub, summer-green	<i>Salix</i> (willow species (osier, willow))
	LSE	Low shrub, broadleaved evergreen	<i>Calluna vulgaris</i> (heather)
			<i>Artemisia</i> (mugwort species)
			Amaranthaceae/ Chenopodiaceae (amaranth family/e.g. goosefoot**)
			Cyperaceae (sedges)
Open land (OL)	GL	Grassland - all herbs	<i>Filipendula</i> (meadowweet)
			Poaceae (grass family)
			<i>Plantago lanceolata</i> (ribwort plantain)
			<i>Rumex acetosa-t</i> (common sorrel and some other <i>Rumex</i> (dock) species)
	AL	Agricultural land - cereals	Cereal-t (all cereals)

---

except *Secale cereale*

(rye))

---

*Secale cereale* (rye)

---

320

## 321 **2.5 REVEALS**

322 REVEALS (Regional Estimates of Vegetation Abundance from Large Sites) is a model that was  
323 developed to estimate regional vegetation cover at a scale of  $10^4$ - $10^5$  km<sup>2</sup> using pollen records from  
324 large lakes (100-500 ha) (Sugita, 2007). REVEALS requires dates, records of pollen counts, relative  
325 pollen productivities of plants, values of fall speed of pollen, and a model of pollen dispersal and  
326 deposition. The output is plant percentage cover with an associated standard error. The REVEALS  
327 model can also be applied on pollen records from multiple small sites (lakes and bogs), the standard  
328 error will however be larger than with pollen data from large lakes (Sugita 2007; Trondman et al.,  
329 2015; Trondman et al., 2016). For use in climate modelling, REVEALS estimates of plant cover are  
330 achieved at a 1° grid scale using all suitable (see below) pollen records available in each grid cell. A  
331 REVEALS land cover reconstruction was previously performed for a large part of Europe  
332 (Trondman et al., 2015). The requirements and criteria for pollen records to be suitable are listed in  
333 Trondman et al. (2015) as well as all details on the pollen data handling and parameter settings for  
334 the REVEALS application (Mazier et al., 2012; Trondman et al., 2015, Appendix S2: The  
335 LandClim protocol). For the purpose of this study, we increased the coverage of the REVEALS  
336 reconstruction southwards to the Mediterranean area and eastwards to western Russia and the  
337 Middle East, and incorporated pollen records from new sites across the entire study region. The  
338 dataset increased from 636 pollen records (Trondman et al., 2015) to 1138 pollen records (Githumbi  
339 et al., 2021).

340

## 341 **2.6 Spatial statistics**



342 The spatial statistics estimation (see Pirzamanbein et al., (2018) and Pirzamanbein et al., (2020) for  
343 a complete description) uses computer intensive statistical inference methods (Roberts & Stramer,  
344 2002; Brooks et al 2011) to interpolate REVEALS model outputs (i.e. gridded pollen-based land-  
345 cover at a 1 degree grid) to all grid cells; providing complete vegetation cover across Europe. The  
346 spatial interpolation is a modified generalized linear mixed model with spatially dependent  
347 residuals. It has three main components:

348

349 1) The vegetation cover is modelled as compositional data (Aitchison, 1986) using a Dirichlet  
350 distribution (the generalized part of the generalized linear mixed model). This ensures that the  
351 interpolated fractions of vegetation cover are between 0 and 1 and sum to 1; thus 2) Large-scale  
352 features in the interpolation are modelled by regressing the REVEALS outputs onto a set of  
353 covariates (the linear component). The covariates used here consist of elevation and potential  
354 vegetation from LPJ-GUESS, driven by the EC-Earth climate model, and adjusted for the KK10  
355 anthropogenic land cover. The regression essentially computes correlations between REVEALS  
356 outputs and covariates and then scales the covariates according to the correlation. Thus, the  
357 regression uses the spatial patterns of the covariates, but **not** their absolute values. A sensitivity  
358 study (Pirzamanbein et al., 2020) showed that the interpolation is reasonably insensitive to different  
359 possible covariates. 3) The spatial mixed effect, modelled using a Gaussian Markov Random Field  
360 (Lindgren et al., 2011), captures any spatial patterns in the REVEALS outputs, which are not found  
361 in the covariates. The final interpolation is subsequently a statistically optimal combination of these  
362 spatial patterns and the covariate information.

363

364 The spatial model provides pollen-based estimates of vegetation cover, and only accounts for  
365 vegetated areas. The final *reconstructed land-cover* (R) is obtained by adjusting the output from the  
366 statistical model with the fraction of bare ground from LPJ-GUESS simulated potential natural  
367 vegetation using EC-Earth derived 6 ka climate data. This adjustment enhances land cover openness

368 in sparsely vegetated areas, such as the OL (open land) fraction of the REVEALS-based vegetation  
369 reconstruction in grids with simulated bare ground, such as in mountainous regions in the Alps and  
370 northern Scandinavia and along northern coasts.

371

## 372 **3 Results**

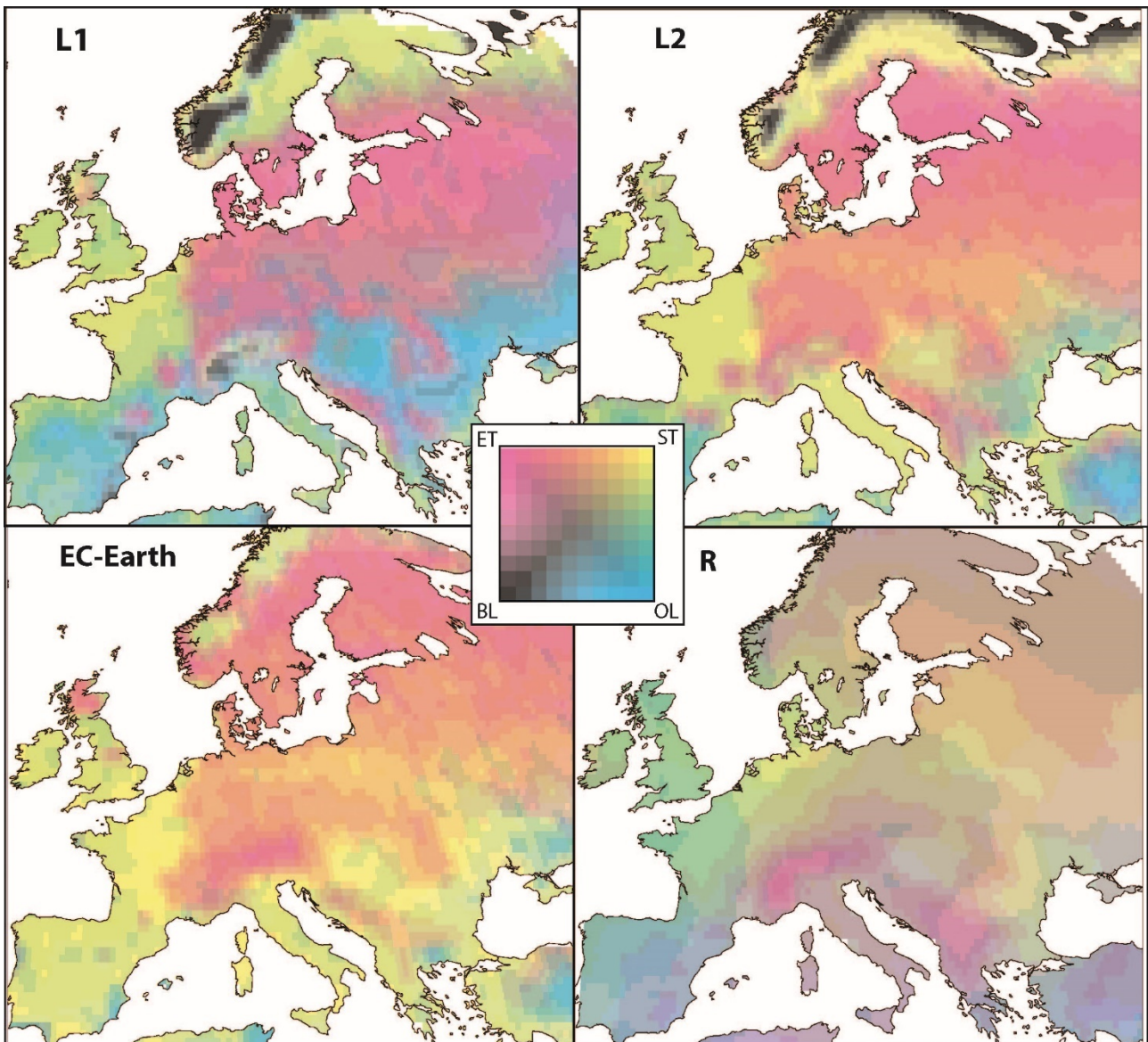
### 373 **3.1 Simulated vegetation**

374 The potential vegetation cover of Europe at 6 ka, simulated by LPJ-GUESS, is dominated by forests  
375 according to all modelled scenarios (Fig. 2). Evergreen trees (ET) prevail in central and eastern  
376 Europe, while summergreen trees (ST) dominate western Europe. The simulated land cover of  
377 southern Europe is largely open, depending on the model scenario. The simulation using the  
378 coarser-scale EC-Earth climate data as the input does not show dominance of bare ground  
379 anywhere. The high-resolution RCM-based simulations L1 and L2 suggest that large parts of the  
380 Scandinavian mountains were covered by very sparse vegetation. This difference between the  
381 global and regional models is related to differences in elevation where the high-resolution RCMs  
382 have higher elevations in the mountainous regions, and therefore also represent colder and less  
383 favourable conditions. This is also indicated by larger fractions of non-vegetated areas in other  
384 mountainous regions including the Alps. There are also important differences between L1 and L2 in  
385 Scandinavia. This is a consequence of the different climate scenarios simulated by RCA4 (L1) and  
386 HCLIM (L2). L1 shows larger areas of bare ground in the mountain range, and a generally more  
387 open landscape in northern Sweden and Finland; while L2 shows more extensive bare ground in the  
388 Kola peninsula (in the far north east of the domain), as well as forests dominated by ET extending  
389 further north.

390

391 The reconstructed land cover (R) shows less latitude-dependant zonal vegetation composition than  
392 model-simulated vegetation across all of Europe. Mixed forests with both ST and ET are dominant,  
393 with ET more abundant in northern and eastern Europe, while ST is more abundant in western

394 Europe. Moreover, R indicates more open land (larger cover of OL) than simulated by LPJ-GUESS,  
395 except in the southernmost regions. Although the EC-Earth/LPJ-GUESS-simulated bare ground has  
396 been accounted for in R, by increasing OL at the expense of ET and ST, the overestimation of ET  
397 (mainly pine), in the Alps, the Scandinavian mountains and northernmost Scandinavia is a pollen-  
398 based bias not entirely corrected by REVEALS (Binney et al., 2011; Trondman et al., 2015), which  
399 is not completely removed.  
400



401  
402 **Figure 2** Composite maps of LPJ-GUESS simulated potential natural vegetation cover using  
403 climate inputs derived from different climate models (L1 – RCA4, L2 - HCLIM, EC-Earth) and  
404 reconstructed vegetation cover (R) of Europe at 6 ka.

405 Legend: ET – evergreen forest; ST– summergreen forest; OL – open landcover; BL – bare ground.

406

407

### 408 **3.2 Simulated climate**

409 Figure 3 shows the simulated differences between 6 ka and PI climate. Here we discuss only the 6k-

410 R runs (based on REVEALS reconstructed vegetation) since they use the most realistic land-cover

411 data. The impact of different vegetation is discussed in section 3.3. In winter, all simulations concur

412 that 6 ka was warmer than the PI period, and all simulations provide a similar pattern, with the

413 smallest differences in temperature at 2 metre over the Iberian Peninsula (0.5-1.5 °C) and the largest

414 in north-eastern Europe (4-7 °C). EC-Earth is in the lower end of this range, showing differences of

415 around 1°C less than RCA4 and around 2 °C less than HCLIM for most of Europe. In parts of

416 Scandinavia and Russia the differences in HCLIM are smaller than in RCA4, and for some

417 locations even smaller than in EC-Earth. In summer the smallest differences are also found over the

418 Iberian Peninsula and western Europe, and the largest differences are found in south-eastern Europe

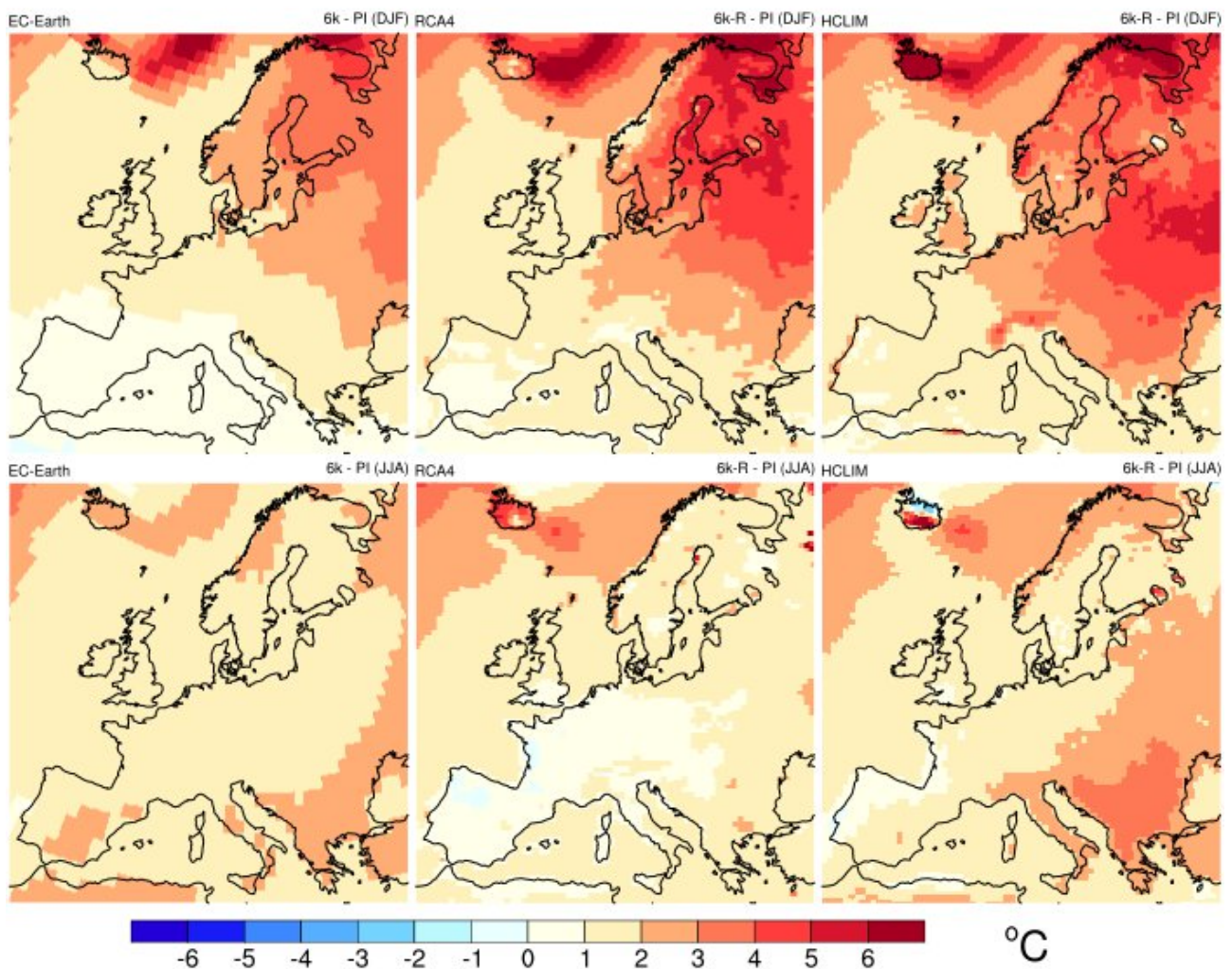
419 as well as in areas close to the sea-ice margin in the far north. The difference between RCA4 and

420 HCLIM is larger in summer, although the temperature pattern is similar in both models. While the

421 temperature differences between 6k-R and PI span 0.5-3.5 °C in HCLIM, the differences in RCA4

422 are close to zero in western Europe, and not more than 2 °C in the southeast. EC-Earth lies between

423 the RCMs with very small variations between parts of Europe.



424

425 **Figure 3** Temperature difference (°C) between 6k-R and PI for winter (DJF, top row) and summer  
426 (JJA, bottom row) for EC-Earth (left), RCA4 (middle) and HCLIM (right).

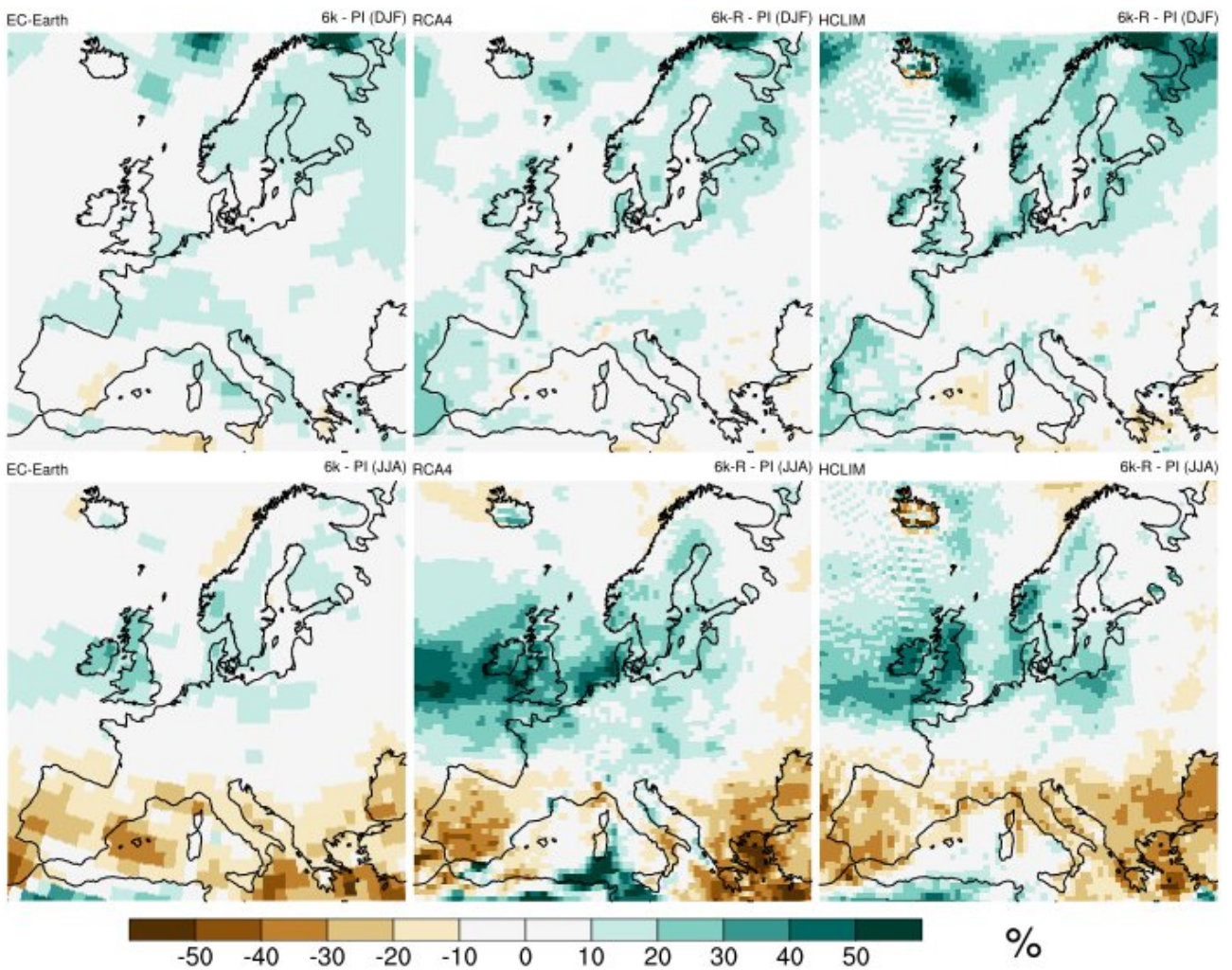
427

428

429 Generally, 6k-R is wetter than PI in winter, especially in western and northern Europe where 6 ka is  
430 10-25 % wetter in all three models (Fig. 4). Some regions in central Europe and the Mediterranean  
431 have small or even negative differences of up to 10 %. In summer, there is a clear distinction

432 between northern and southern Europe. In most of northern Europe 6 ka is wetter by more than  
433 25 %, whereas in large parts of southern Europe 6 ka is at least 25 % drier. The precipitation  
434 patterns are similar in all three models, although with higher amplitudes in the RCMs, which  
435 suggests that precipitation is mostly governed by the driving GCM and less by the RCMs. This  
436 strong dependency of precipitation changes on the large-scale circulation as given by the GCMs is a  
437 well-known feature seen also in projections of future climate change (e.g. Kjellström et al., 2018;  
438 Christensen and Kjellström, 2020).

439



440

441 **Figure 4** Precipitation difference (%) between 6k-R and PI for winter (DJF, top row) and summer  
442 (JJA, bottom row) for EC-Earth (left), RCA4 (middle) and HCLIM (right).

443

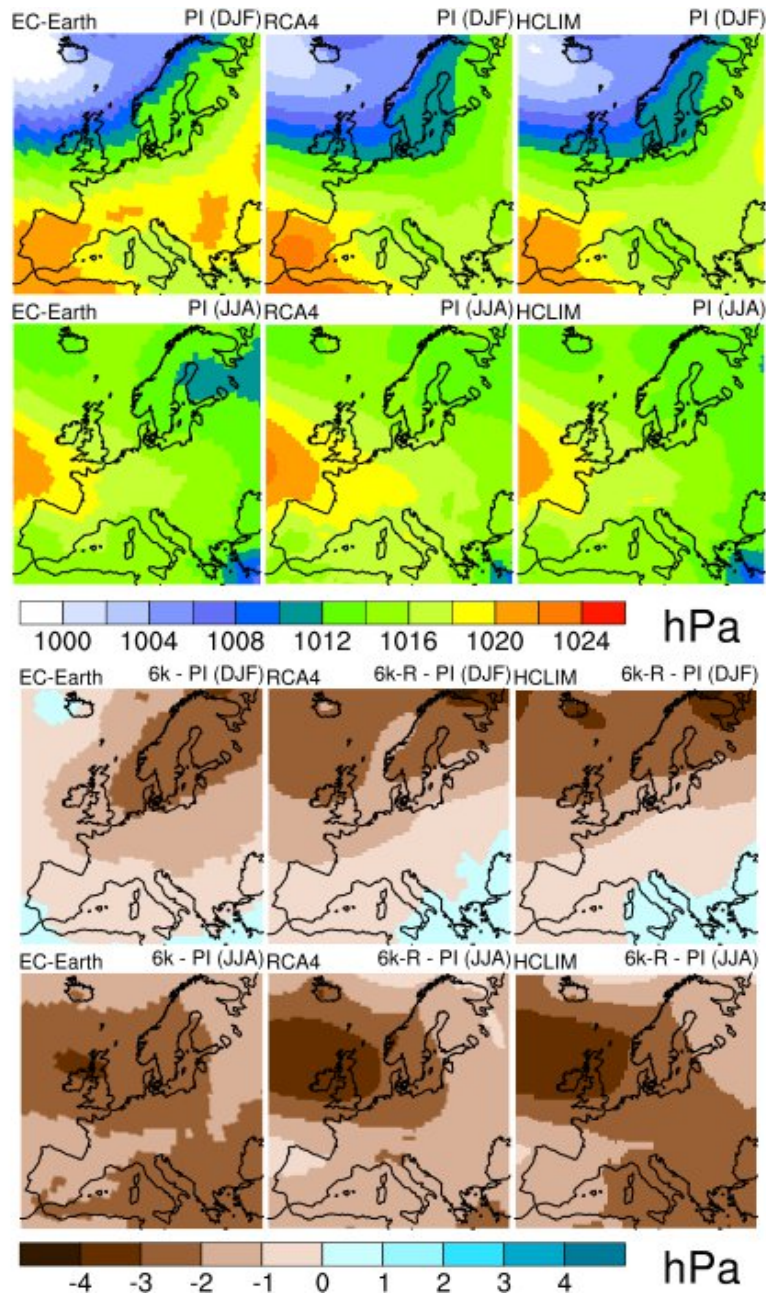
444 Figure 5 shows sea level pressure (SLP) at PI and the difference between 6ka and PI. In winter the  
445 SLP over Scandinavia is clearly lower in the RCMs compared to in EC-Earth. This indicates that  
446 low-pressure systems have a stronger influence in eastern parts of the Atlantic sector in the RCMs  
447 than in EC-Earth. Comparing the two time periods it is clear that SLP is lower at 6 ka over  
448 Scandinavia and northeastern Europe, which implies enhanced cyclone activity. This tendency of  
449 lower 6 ka SLP differs between EC-Earth and the RCMs: it is stronger in EC-Earth over the  
450 easternmost parts of the domain while both RCMs show stronger negative anomalies over large  
451 parts of the north Atlantic. Such differences between the RCMs and the driving global climate  
452 model may partly explain differences in precipitation anomalies between the models. For instance,  
453 the stronger SLP anomaly over the easternmost part of the domain in EC-Earth compared to the  
454 RCMs may be related to the larger positive precipitation anomaly in that region (cf. Fig. 5). The  
455 RCMs, on the other hand, show that stronger precipitation anomalies are further north, including the  
456 Baltic Sea area. Over parts of the North Atlantic, the RCMs indicate more precipitation associated  
457 with lower SLP.

458

459 In summer, the Icelandic low is located further to the south at 6 ka, which means stronger westerlies  
460 on average and increased low pressure activity over the North Atlantic and western Europe. This is  
461 reflected in the higher precipitation seen at 6 ka in western Europe (cf. Fig. 4). The larger  
462 precipitation anomalies seen in the RCMs correspond to larger pressure anomalies. SLP is also  
463 slightly lower in the Mediterranean region. In this region, higher temperatures lead to a decrease in  
464 soil moisture, and therefore do not lead to increased precipitation. In the far north, on the other  
465 hand, the somewhat higher sea level pressure at 6 ka is indicative of a weaker pressure gradient and,

466 consequently, less cyclonic activity which can partly be seen as reduced rainfall in some areas –  
467 close to the Norwegian coast and west of Iceland.

468



469

470 **Figure 5** PI sea level pressure (hPa) in winter (DJF, first row) and summer (JJA, second row).

471 Difference in sea level pressure (hPa) between 6k-R and PI in winter (DJF, third row) and summer

472 (JJA, fourth row). EC-Earth (left), RCA4 (middle) and HCLIM (right).

473

474 **3.3 Climate response to changes in vegetation – the importance of ALCC**



475 In this section the 6k-R runs described in section 3.2 will be used as the reference and compared to  
476 the 6k-L1 and 6k-L2 runs, i.e. we discuss the climate difference (6k-L1) – (6k-R) and (6k-L2) –  
477 (6k-R), abbreviated L1-R and L2-R below (Table 1). In this way we will see how RCA4 and  
478 HCLIM respond to the changes in vegetation indicated by Fig. 2. Here we show the surface  
479 temperature instead of the diagnostic 2 m-temperature, which is defined in different ways  
480 depending on the model, and may represent different things (Breil et al., 2020). Surface temperature  
481 has a common definition, and correlates better to differences in radiation and heat fluxes.  
482 Differences are tested using a student's t-test with Bonferoni (1936) correction for multiple testing.  
483 The resulting procedure has a 5% family-wise error rate, i.e. the probability of one or more false  
484 positives among all grid cells is 5%; instead of the 5% false positive rate for each individual grid  
485 cell obtained when no correction is applied.

486

487 L1-R differences in winter surface temperatures are very small in both RCA4 and HCLIM  
488 simulations in western and southern Europe, which is expected given the small differences in L1  
489 and R vegetation in these regions. L1-R temperature differences are within  $\pm 0.5^{\circ}\text{C}$ , if at all  
490 significant. In areas with more pronounced L1-R differences in land cover, such as central and  
491 north-eastern Europe and the Alps, the L1-R differences in winter temperature are larger, up to  $1^{\circ}\text{C}$   
492 in RCA4 and  $2^{\circ}\text{C}$  in HCLIM (Fig. 6). In Scandinavia and to some extent the Iberian Peninsula, 6k-  
493 L1 and 6k-L2 are colder than 6k-R. The response in 6k-L2 in HCLIM is particularly strong, up to  
494  $3^{\circ}\text{C}$  colder.

495 For both L1 and L2 the albedo difference is similar, but not the same, in RCA4 and HCLIM. The  
496 most notable differences are found around the Mediterranean, where the L1-R and L2-R albedo  
497 difference is negative in RCA4 and positive in HCLIM (Fig. 7). The differences in winter and  
498 spring surface temperatures are correlated with the differences in albedo (Fig. 7). Surface  
499 temperatures are generally reduced where albedo is increased and increased where albedo is  
500 reduced. RCA4 is not very sensitive to differences in albedo between L1, L2 and R in winter, and

501 shows significant L1-R and L2-R differences in temperature only in the Alps and the Carpathians.  
502 Since these are mountainous regions, it seems likely that the temperature differences are connected  
503 to snow cover rather than directly to the albedo of different vegetation types. Landscapes that are  
504 more open are more readily covered with snow, which means that albedo is extra high during the  
505 snow season. This will further increase the difference in winter and spring albedo between forests  
506 and open land; which in turn increases the difference in temperature (e.g. Gao et al., 2014;  
507 Strandberg & Kjellström, 2019; Davin et al., 2020). HCLIM shows a stronger response in winter  
508 temperature. Both L1-R and L2-R differences are 0.5-1 °C in large parts of central and eastern  
509 Europe. The largest differences in albedo are seen in the Scandinavian mountains. In the L2  
510 vegetation a large part of the Scandinavian mountain range is non-vegetated (Fig. 2). Therefore, the  
511 L2-R albedo differences, and thus the L2-R temperature differences, are larger than the L1-R  
512 differences. The L1 vegetation used in the 6k-L1 simulations has larger vegetation-covered areas in  
513 the Scandinavian mountain range. At high latitudes the albedo effect is strongest in spring, since the  
514 snow season is longer and the winter insolation is weak. In HCLIM 6k-L1 is 0.5-1.5°C warmer than  
515 6k-R in central Scandinavia in spring (March-May, see Fig. S1 in Appendix A), corresponding to a  
516 negative L1-R albedo difference in the region. 6k-L2 is 1-3°C colder than 6k-R in the Scandinavian  
517 mountain range, corresponding to a positive L2-R albedo difference in this region (Fig. S1 in  
518 Appendix A).

519

520 In summer, RCA4 and HCLIM respond differently to changes in vegetation (Fig. 8). The  
521 differences are small, but significant for large parts of Europe. For RCA4, both 6k-L1 and 6k-L2  
522 are around 0.5 °C colder than 6k-R. The only large difference between 6k-L1 and 6k-L2 for RCA4  
523 is over the Scandinavian mountains. This region is less forested in 6k-L2 than in 6k-L1, which leads  
524 to even larger temperature differences compared to 6k-R, which shows the smallest fraction of open  
525 land in this area. In HCLIM, both 6k-L1 and 6k-L2 are warmer than 6k-R in summer in central and

526 eastern Europe, and colder in the south and north. The differences are rather small, mostly within  
527  $\pm 0.5$  °C.

528

529 Differences in summer surface temperature are opposite to differences in evapotranspiration in both  
530 RCA4 and HCLIM (Fig. 9). A larger forest fraction gives increased evapotranspiration, which  
531 lowers surface temperature. Conversely, a smaller forest fraction gives decreased  
532 evapotranspiration, which elevates the surface temperature. In southern Europe 6k-L1 and 6k-L2  
533 are colder than 6k-R due to positive L1-R and L2-R differences in evapotranspiration from the  
534 denser forest in 6k-L1 and 6k-L2 compared to 6k-R; 5-15 % more evapotranspiration in HCLIM  
535 and up to 20 % more in RCA4. In northern Scandinavia, 6k-L1 and 6k-L2 are colder despite the  
536 smaller forest fraction and lower evapotranspiration. The mountain regions do sometimes have  
537 snow during summer, which means that albedo is also an important factor in summer (JJA). In  
538 addition, the cold climate generally leads to reduced evapotranspiration and thus reduces the  
539 potential for changes in land cover to affect temperature.

540

541 Significant L1-R and L2-R summer evapotranspiration differences are seen in northern Scandinavia  
542 and around the Mediterranean. In Scandinavia, less evapotranspiration in L1 and L2 is connected to  
543 the larger degree of open land. In the South, only RCA4 shows large-scale significant differences.  
544 Positive L1-R and L2-R evaporation differences are connected to more extensive forest fractions in  
545 this region. Strandberg et al. (2014) noted that the albedo effect also dominates in southern Europe  
546 in summer in their study based on RCA3. The already dry soils prevent changes in  
547 evapotranspiration regardless of changes in land cover. We see a tendency towards such an effect in  
548 small areas in the southwestern part of the Iberian Peninsula in RCA4 and parts of Italy and  
549 southwestern Iberia in HCLIM. This effect is suggested to be stronger when the forest fraction is  
550 reduced to below 20 % (Strandberg et al., 2014), which is not the case in these simulations.

551

552 The studied vegetation changes have only little effect on precipitation (Figs. S2 & S3 in Appendix  
 553 A). With larger forest fraction, the surface roughness is higher. The increased friction leads to  
 554 stronger convergence, which in turn leads to more precipitation (Belušić et al., 2019). There is such  
 555 a tendency, but differences in precipitation are essentially insignificant everywhere.  
 556

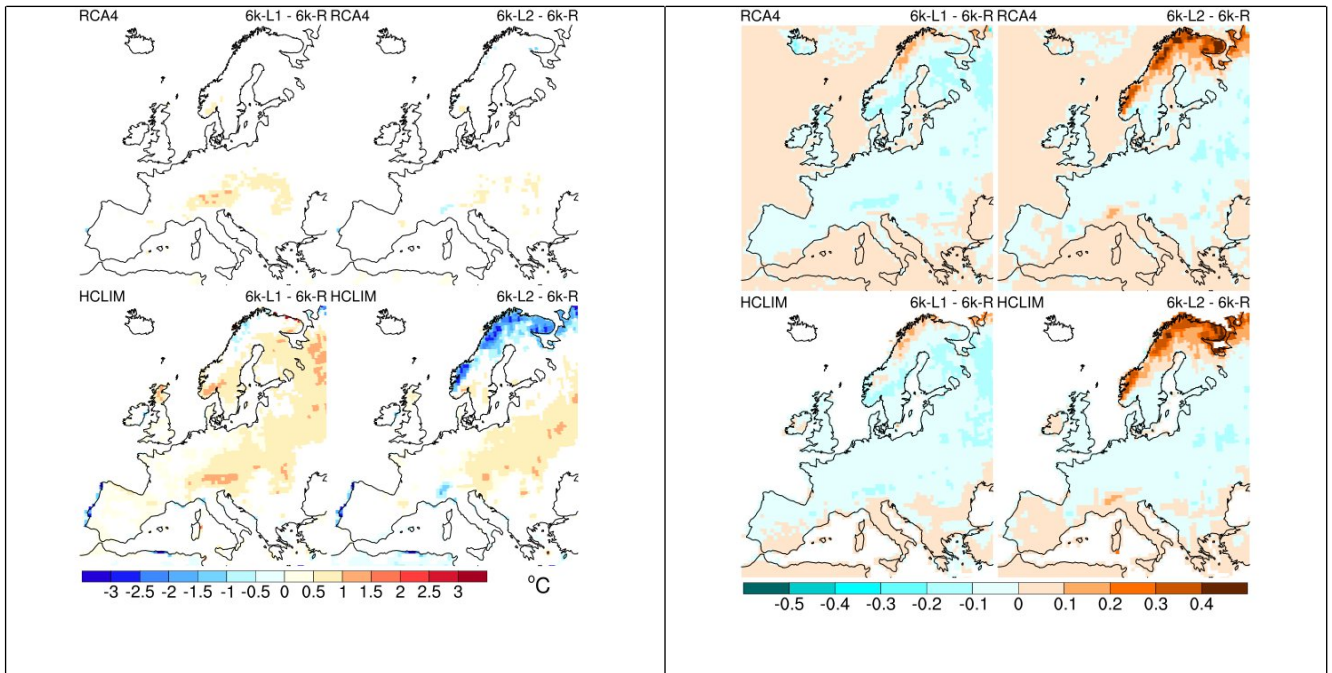


**Figure 6** Difference in surface temperature (°C) in winter for RCA4 (top row) and HCLIM (bottom row) between 6k-L1 and 6k-R (left column) and 6k-L2 and 6k-R (right column). Only grid cells that show a significant difference on a 0.05 level are coloured.

**Fig 7** Difference in albedo in winter for RCA4 (top row) and HCLIM (bottom row) between 6k-L1 and 6k-R (left column) and 6k-L2 and 6k-R (right column). Only grid cells that show a significant difference on a 0.05 level are coloured.

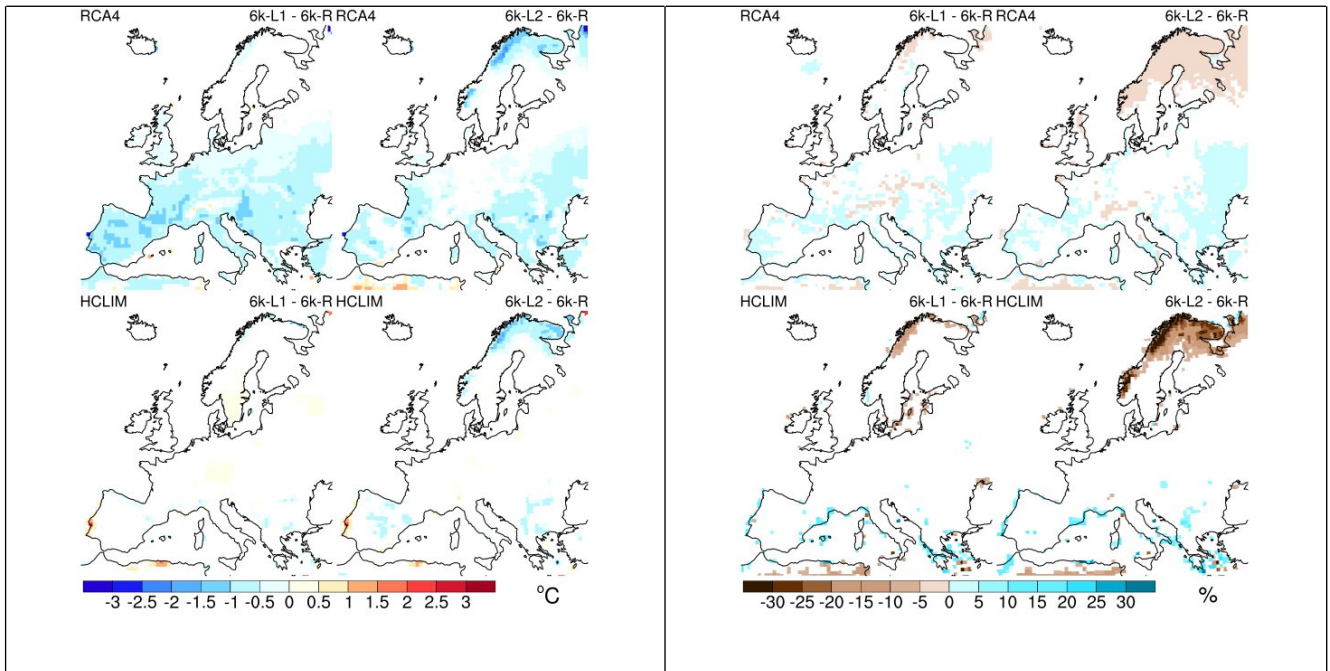


**Fig 8** Difference in surface temperature (°C) in summer for RCA4 (top row) and HCLIM (bottom row) between 6k-L1 and 6k-R (left column) and 6k-L2 and 6k-R (right column). Only grid cells that show a significant difference on a 0.05 level are coloured

**Fig 9** Difference in evapotranspiration (%) in summer for RCA4 (top row) and HCLIM (bottom row) between 6k-L1 and 6k-R (left column) and 6k-L2 and 6k-R (right column). Only grid cells that show a significant difference on a 0.05 level are coloured.

557

558

559

## 560 **4 Discussion**

### 561 **4.1 Differences in land-cover descriptions – cause and effects**

562 Simulated (L1 and L2) and reconstructed (R) land cover exhibit clear compositional differences. It  
 563 must be kept in mind that the DVM simulated potential natural vegetation in this study is entirely  
 564 determined by prescribed simulated climate, i.e. the simulations do not account for the effects of  
 565 LULCC. The reconstructed land cover, in contrast, is a pollen-based reconstruction of the actual  
 566 vegetation, that is a product of complex interactions between several natural and anthropogenic  
 567 factors including the actual climate. However, LULCC do not explain all differences between R and

568 L1 or L2. L1 and L2 are two sets of DVM simulated natural potential vegetation differing only in  
569 input climate that is taken from two different RCMs. The pollen-based reconstructed land cover R is  
570 a result from the actual climate at 6 ka and human impact on vegetation. Thus, differences between  
571 R and L1 or L2 can also be due to differences between the actual climate and the RCM-simulated  
572 climates. This implies that some differences can be due to LULCC while others can be due to  
573 differences between simulated and actual climates and to weaknesses in the applied methods. The  
574 R land cover suggests that the largest LULCC at 6 ka occurred in southern and western Europe, in  
575 agreement with an earlier REVEALS reconstruction of land cover in Europe (Trondman et al.,  
576 2015) and with LULCC scenarios (Kaplan et al., 2010, Kaplan et al., 2017). Thus, it is unlikely that  
577 the differences between R and L1 or L2 in Scandinavia mainly are caused by LULCC. Therefore,  
578 the difference in climate in this region between 6k-R and 6k-L1 or 6k-L2 is most probably not an  
579 effect of anthropogenic changes in this part of Europe, but rather an effect of how 6 ka climate is  
580 represented in LPJ-GUESS and REVEALS. In southern Europe, however, differences in climate  
581 might be a response to LULCC. The 6 ka – PI difference in summer temperature is amplified by 0.5  
582 degrees when R vegetation is used. The extent of this effect is highly model dependent. The RCA4-  
583 simulated 6k-R climate is warmer in most of southern Europe, while the HCLIM-simulated 6k-R  
584 climate exhibit significant temperature differences only in parts of the Iberian and Balkan  
585 Peninsulas.

586

#### 587 **4.2 RCM simulated climates compared to proxies**

588 In the comparison between model results and reconstructed climate, we first exclude purely pollen  
589 based proxies, as our results are based on pollen data to some extent. This allows us to avoid  
590 circular reasoning in model-data comparison. Studies of diatoms (Korhola et al., 2000; Rosén et al.,  
591 2001; Bigler et al., 2006; Heinrichs et al., 2006; Shala et al., 2017), tree rings (Grudd, 2002; Helama  
592 et al., 2002) and chironomids (Rosén et al., 2001; Bigler et al., 2003; Hammarlund et al., 2004;  
593 Laroque and Hall, 2004; Velle et al., 2005; Heinrichs et al., 2008; Luoto et al., 2010; Shala et al.,

2017) indicate a 6 ka – PI difference in summer temperature of 0.5–2 °C in Scandinavia, which corresponds with our simulations (cf. Fig. 3). Evidence from the presence of Mediterranean ostracods in the coastal waters of Denmark suggests that winter temperatures at 6 ka were up to 4–5 °C above present (Vork and Thomsen, 1996). Our model results do not show such a large temperature increase, but it is nevertheless clear that the difference 6 ka – PI is larger in winter than in summer. Non-pollen proxies are scarce in central Europe. Diaconou et al. (2017) report around 0.5 °C colder summers in Romania based on chironomids, while Larocque-Tobler et al. (2009) and Heiri and Lotter (2005) found 0.5-1 °C warmer summers in Switzerland. Persoiu et al. (2017) do not present quantitative estimates, but based on stable isotope analysis they report warmer winters in central Europe and colder winters in eastern Europe. This is somewhat in conflict with our model results as 6 ka is simulated to be warmer than PI during all seasons for practically all of Europe. Proxy records of relative precipitation indicate a drier climate at 6 ka than at PI in Scandinavia (Digerfeldt, 1988; Ikonen, 1993; Snowball and Sandgren, 1996; Hammarlund et al., 2003; Borgmark, 2005; Olsen et al., 2010), northern Germany (Niggeman et al., 2003), the UK (Hughes et al., 2000) and the western Mediterranean (Walczak et al., 2015; Persoiu et al. 2017), while there is no detectable difference in the Alps (Magny, 2004) and wetter conditions in eastern Europe (Persoiu et al., 2017; Galka and Apolinarska 2014). This contrasts with the present model results that show wetter conditions in the north and west and drier in the south. This is not explained by the fact that many estimates based on biological proxies reflect effective precipitation (the relationship between precipitation and evapotranspiration). The models yield small differences or increases in effective precipitation, depending on model and season. The fact that the models indicate warmer and wetter conditions than the proxies is a general feature of the CMIP5/PMIP3 global simulations of the mid-Holocene PI climates (Harrison et al., 2015; Barthlein et al., 2017). The accepted explanation for this is the too weak zonal flows, and thus too weak moisture transport in the GCMs; which is reasonable given the approximate 2°×2° resolution in PMIP3.

619

620 The only spatially extensive reconstructions are based on pollen data. Therefore, after having  
621 compared with other independent proxy data above, we make a deviation from the principle of not  
622 comparing with pollen-based data. This is done bearing in mind that the R vegetation in our  
623 simulations is based on pollen data transformed into vegetation cover. Mauri et al. (2014)  
624 (henceforth M14) presented a gridded reconstruction of 6k-PI for all of Europe. M14 reveals the  
625 largest temperature difference in Scandinavia (especially in winter), and a gradient with smaller  
626 differences between 6 ka and PI towards the south west. In M14, 6 ka is colder than PI over the  
627 Iberian Peninsula and most of the Mediterranean. Our simulations show a similar pattern in  
628 northern Europe. In southern Europe the differences are small and mostly positive; other than for a  
629 few regions in RCA4 in summer (Fig. 3). Precipitation conditions in winter are generally wetter in  
630 the northeast, in line with our simulations, but drier in the west, which is in disagreement with our  
631 results. In summer M14 identified a near opposite pattern as those in our simulations with drier  
632 conditions in Scandinavia and wetter in the southeast of Europe.

633

634 The result showing that 6 ka was warmer and wetter (at least in winter) than PI in Fennoscandia is a  
635 robust outcome supported by most proxies and climate models. For the rest of Europe, the results  
636 presented here do not agree as clearly with other proxies and reconstructions. However, proxy  
637 reconstructions are sparse for central and southern Europe and also less consistent with each other.  
638 Both Perciou et al. (2017) and Peyron et al. (2017) state that the Mediterranean 6 ka climate was  
639 mostly wetter than PI, but with large geographical variation. This is in some conflict with the  
640 precipitation differences presented in this study, which are mostly drier.

641

#### 642 **4.3 Differences between 6 ka and PI climates - comparison with previous studies**

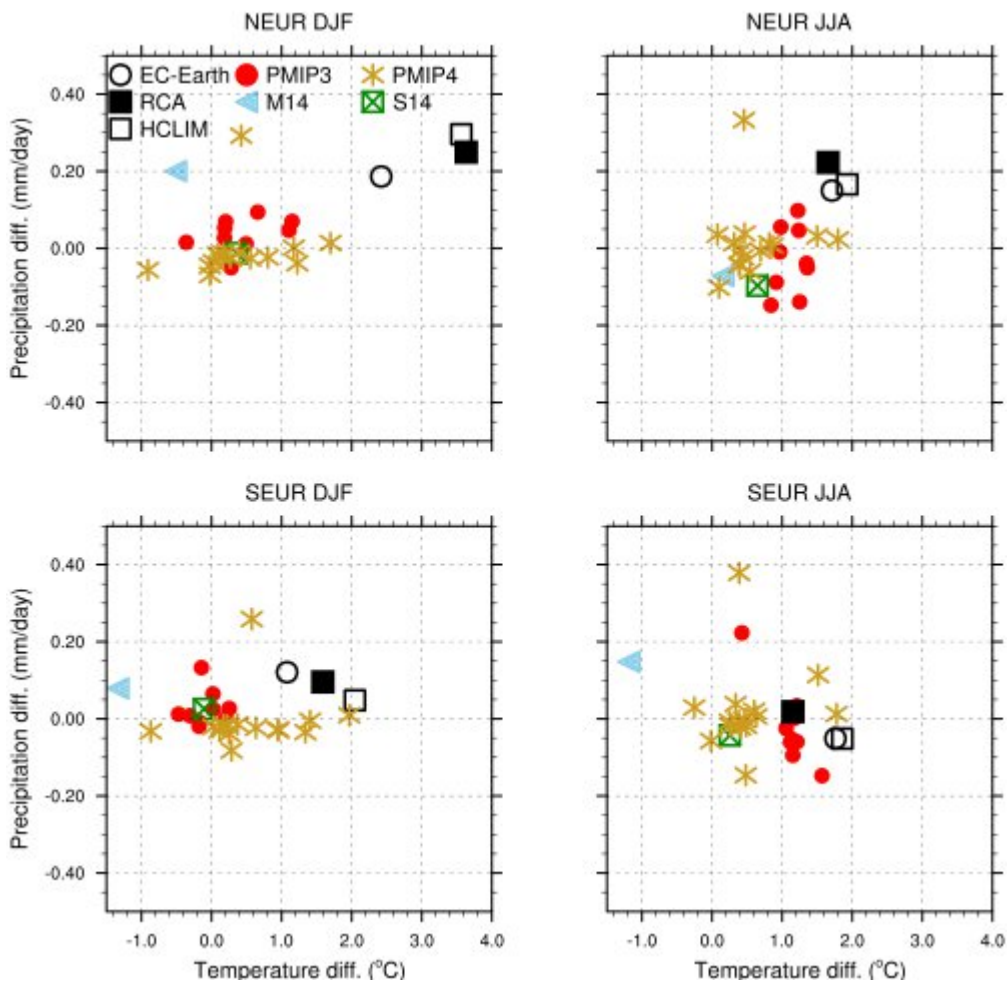
643 The simulations presented here are compared with results from 9 PMIP3 models (Braconnot et al.,  
644 2012) as well as data from M14 and Strandberg et al. (2014, henceforth S14). The PMIP3 models  
645 used are: BCC-CSM1-1 (Wu et al., 2014); CNRM-CM5 (Voltaire et al., 2012); CSIRO-Mk3-6-0



646 (Rotstayn et al., 2012); FGOALS-GS (Li et al., 2013); GISS-E2-R (Schmidt et al., 2014); IPSL-  
647 CM5A-LR (Dufresne et al., 2013); MIROC-ESM (Watanabe et al., 2011); MPI-ESM-P (Stevens et  
648 al., 2013); and MRI-CGCM3 (Yukimoto et al., 2012). S14 simulated 6 ka climate with an approach  
649 similar to the present, for example, by using RCA3 in combination with LPJ-GUESS.

650

651 Figure 10 shows the differences in temperature and precipitation between 6 ka and PI for northern  
652 Europe (NEUR, -10 - 34 E, 50 - 70 N) and southern Europe (SEUR, -8 - 24 E, 35 - 50 N) from the  
653 GCM and RCMs (6k-R) used in this study, the PMIP3 and PMIP4 GCMs, the S14 RCM and the  
654 reconstruction from M14. There is some spread between the PMIP3 models and a larger spread  
655 between PMIP4 models, especially for temperature. The difference in precipitation between 6 ka  
656 and PI is at the most between -0.2 mm/day and +0.2 mm/day, with the exception of one PMIP4  
657 model that reaches up to 0.4 mm/day. The difference in temperature is at the most between -1 °C  
658 and 2 °C. The models used here, EC-Earth3-LR, RCA4 and HCLIM give a considerably larger 6  
659 ka-PI difference than the PMIP3 models, but is within the range of PMIP4 for except for winter in  
660 northern Europe. The temperature difference is never less than 1 °C, and in northern European  
661 winter this is almost 4 °C. In northern Europe, the precipitation differences are also considerably  
662 larger. RCA4 and HCLIM are in close agreement with the driving EC-Earth, but are not identical.  
663 Using different models would give different results, but not change the overall conclusions,  
664 although within the PMIP4 ensemble EC-Earth-LR is the model that shows the largest winter  
665 warming in northern Europe. In any case, it is difficult to say which model would be the best  
666 representing 6 ka climate conditions. Brierly et al. (2020) report a PMIP4 6 ka – PI precipitation  
667 difference similar to PMIP3 in Europe. For temperature, Brierly et al. (2020) show that PMIP3 and  
668 PMIP4 are similar; the largest exception is that the difference in summer temperature between 6 ka  
669 and PI in northern Europe is smaller in PMIP4 than in PMIP3.



670

671 **Figure 10.** Difference in temperature (°C) and precipitation (mm/day) between 6 ka and PI (6 ka –  
 672 PI) in northern Europe (NEUR, top row) and southern Europe (SEUR, bottom row) for winter (DJF,  
 673 left column) and summer (JJA, right column). The simulations in this study using 6k-R vegetation  
 674 are represented by open circles (EC-Earth3-LR), filled squares (RCA4) and open squares (HCLIM).  
 675 Red dots represent PMIP3 models, gold stars PMIP4 models, blue triangles data show from Mauri  
 676 et al. (2014, M14) and green crossed squares show data from Strandberg et al. (2014, S14).

677

678 S14 simulated a 6 ka climate that was warmer than PI by 2-3 °C at the most (the largest differences  
 679 were identified in northern Europe in winter and southern Europe in summer). For winter, we obtain  
 680 a similar temperature difference between 6 ka and PI as S14 with a gradient from the northeast,  
 681 which is around 3 °C warmer than the southwest where the 6 ka-PI difference is close to zero. In  
 682 summer, we identify a small positive 6 ka-PI difference in the southwest, where S14 show a 6 ka

683 climate that is up to 3 °C warmer than PI. Since RCA3 and the driving ECHO-G in S14 simulate  
684 similar climates (Fig. 12 in S14), the differences between S14 and the present study are mostly  
685 explained by the different driving GCMs (EC-Earth in this study). For precipitation, the current  
686 results agree with S14 in terms of wetter winter conditions at 6 ka than PI in the north and south and  
687 6 ka-PI differences in precipitation close to zero in central Europe. Contrastingly, the results are  
688 almost opposite for summer precipitation. While in this study 6 ka is characterized by wetter  
689 conditions than PI in the north and drier in the south, S14 identified drier conditions in the north and  
690 somewhat wetter in the southeast. Russo & Cubash. (2016, R16) simulated the 6 ka-PI difference by  
691 using the regional climate model COSMO-CLM forced by ECHO-G (same GCM run as in S14).  
692 For winter they simulated warmer 6 ka conditions in Scandinavia and the British Isles, and colder  
693 conditions in the southeast of Europe. The results of the present study match the clearly warmer  
694 conditions in Scandinavia and the small 6 ka-PI differences over the Iberian Peninsula. For summer,  
695 R16 simulated warmer conditions across Europe at 6 ka comparable to both S14 and the present  
696 study, but without any large variations between different parts of Europe.

697

698 Figure 10 summarizes the differences between 6 ka and PI climates from the studies described  
699 above. All models agree that 6 ka was warmer than PI with the possible exception of southern  
700 European winter where the PMIP3 ensemble and S14 is close to 0 °C. 6 ka is mostly wetter in  
701 winter, while the summer precipitation differences are evenly spread around 0 mm/day. The only  
702 dataset providing proxy-based area averages is M14. For precipitation, M14 is within the spread of  
703 the models. For temperature, M14 is clearly different. In M14, 6k is colder than PI in large parts of  
704 southern Europe. This obvious mismatch between model simulations and reconstructions points to  
705 the issue of the ‘Holocene temperature conundrum’ (HTC, Liu et al., 2014; Bader et al., 2020).  
706 There are regions with major discrepancies between simulated and reconstructed climates across the  
707 globe (Mauri et al., 2014; Harrison et al., 2015; Bartlein et al., 2017). Our result support the idea  
708 that 6 ka was clearly warmer than PI in Europe. The differences between the experiments in this

709 study, however, are minor compared to the differences to other studies. The inclusion of LULCC in  
710 the simulations does not affect this comparison. This shows how the simulated climate is highly  
711 dependent on the models used, especially when forcing conditions are less constrained compared to  
712 present climate.

713

#### 714 **4.4 Robustness of the results**

715 Simulated climate scenarios depend on the climate model(s) used, but the response to differences in  
716 vegetation can also differ significantly between models. Natural internal variability may, therefore,  
717 be a reason for why our results differ from other model studies or from reconstructions based on  
718 proxy data. For current climate conditions, Davin et al. (2020) and Breil et al. (2020) studied the  
719 response to idealized vegetation changes in several RCMs (of which RCA4 was one). All models  
720 agree on the response in albedo and temperature in winter, but in summer the response in heat flux  
721 and temperature, for example, can have different signs. As an example, Russo et al (2021) show that  
722 a RCM can be sensitive to perturbations of the soil moisture, and that land-surface interactions can  
723 explain some of the discrepancies between models and proxies for mid-Holocene summer  
724 temperature in Europe. We would have reached different results if we had used other models. We  
725 try to limit the impacts by using two models with different model physics. We can, to some extent,  
726 describe uncertainty associated with responses to vegetation changes due to model physics, as we  
727 get the same kind of different responses as Davin et al. (2020) and Breil et al. (2020). However, we  
728 acknowledge that we do not represent the full uncertainty and envisage future more comprehensive  
729 studies including a larger variety of climate models to better assess these differences.

730 Summer insolation at 50°N was around 25 W/m<sup>2</sup> higher at 6 ka than at PI while winter insolation  
731 was 5-10 W/m<sup>2</sup> lower (Fischer and Jungclaus, 2011; Xu et al., 2020). Insolation changes explain  
732 differences between 6 ka and PI climate in summer (e.g. Russo and Cubash, 2016), although  
733 alterations in atmospheric circulation may also impact climate (e.g. Mauri et al., 2014). These  
734 differences in insolation are included in EC-Earth, but not explicitly in the RCMs. As lateral

735 boundary conditions and sea surface conditions used in the RCMs are taken from EC-Earth, the  
736 resulting climate in the RCMs indirectly takes into account part of the differences in insolation  
737 between the two periods. Similar inconsistencies between RCMs and their driving GCMs has been  
738 discussed for other forcing agents and other time periods. Differences between present-day and  
739 future climate conditions in RCMs with constant concentrations of greenhouse gases or aerosols has  
740 been shown to differ from that of their driving GCMs where these are changed with time (e.g. Jerez  
741 et al., 2018; Boé et al., 2020). From our results we note that the RCMs have smaller temperature  
742 differences than EC-Earth in western Europe in summer (Fig. 3), which could potentially be a result  
743 of the smaller insolation differences. For eastern Europe the results are ambiguous, with RCA4  
744 showing smaller temperature differences compared to EC-Earth while HCLIM shows larger  
745 differences. These differences indicate that the results are sensitive not only to changes in forcing  
746 factors, but also model-specific formulations of physical processes, resulting in different feedback.  
747 For most ocean areas differences between EC-Earth and the RCMs are small, as the RCMs are  
748 strongly governed by the EC-Earth sea-surface temperatures. We conclude that the missing  
749 description of accurate insolation at 6 ka in the RCMs affects the simulated 6 ka climate. For parts  
750 of the domain, this has likely an impact on the results. Determining the extent of this impact, and  
751 how it may differ between different seasons and locations, is beyond the scope of this study and  
752 requires separate further work.

753 Different insolation could potentially also affect the simulated land cover since insolation has a  
754 direct effect on vegetation. Figure 2 shows vegetation simulated using RCM climate and present  
755 insolation (L1 & L2), vegetation simulated using GCM climate and 6 ka insolation (EC-Earth) and  
756 reconstructed vegetation (R). The differences between L1 and L2 tell us that simulated vegetation  
757 can be different even with the same insolation, because of differences in temperature and  
758 precipitation. Differences to the EC-Earth and R vegetation are the result of the forcing climate and  
759 insolation (and, in the case of reconstructed vegetation, the method used). It seems that the

760 simulated vegetation is more affected by climate than insolation, but we have to acknowledge it as  
761 an uncertainty and suggest assessing sensitivity in vegetation models as a topic for future work.

762

763

## 764 **5 Conclusions**

765 This study describes mid-Holocene (at 6 ka) vegetation and climate as simulated by one GCM, two  
766 RCMs, one DVM and according to one reconstruction of 6 ka vegetation based on pollen data,  
767 statistical interpolation methods and climate model results, which indicates how climate is  
768 influenced by vegetation and LULCC, and how sensitive RCMs are to differences in land cover.

769

770 The models simulate a 6 ka climate that was warmer than PI climate. The largest differences are  
771 seen in Scandinavia in winter where the simulated 6 ka climate is 2-4 °C warmer than PI, a signal  
772 that is shared with proxy data and previous model studies. In summer, the difference between the  
773 simulated 6 ka and PI climates is smaller (0-3 °C) with the smallest differences in the southwest of  
774 Europe. The simulated 6 ka climate is wetter than PI by 10-30 % in the north and the west. Around  
775 the Mediterranean, the simulated 6 ka climate is up to 20 % drier in summer, but with a  
776 precipitation level similar to PI in winter. There is less agreement with other proxy records for  
777 precipitation, but the proxy datasets are also less consistent with one another. The PMIP3 ensemble  
778 also have members that give a positive 6 ka – PI precipitation difference as well as negative. There  
779 is at least some agreement between models and proxies regarding wetter 6 ka conditions in  
780 Scandinavia during winter, while for summer, models and proxies reveal opposite signals. The  
781 signal of a generally warmer 6 ka shown in this study matches other model studies (even though the  
782 magnitude of the difference is unusually large here), but not all proxy reconstructions. The  
783 mismatch between models and proxies connects to the issue of the HTC. This study cannot be used  
784 to make inferences about global temperature or temperature trends throughout the Holocene, but it  
785 clearly supports the notion of 6 ka being warmer (and wetter) than PI in Europe.

786

787 Simulated potential vegetation is dominated by forests: evergreen coniferous forests dominate in  
788 central and eastern Europe, while deciduous broadleaved forests dominate western Europe.

789 Reconstructed land cover, however, shows mixed forests in northern and eastern Europe, and  
790 deciduous broadleaved forests in western Europe. Furthermore, compared to simulated potential  
791 natural vegetation, reconstructed vegetation cover is considerably more open in most of Europe.

792

793 The choice of vegetation has a significant impact on the simulated temperature. Winter and spring  
794 temperatures are closely related to albedo, which is largely the same in both RCMs, and which is  
795 strongly affected by vegetation in both. In summer, the RCMs used in this study respond somewhat  
796 differently to vegetation differences, showing that not only the choice of land cover, but also the  
797 choice of model, is important for the simulated climate. Summer temperatures are strongly related  
798 to differences in heat fluxes between the atmosphere and the ground. Since the response in heat  
799 fluxes to differences in land cover depends on model physics, it is more likely that models respond  
800 differently in summer than in winter. HCLIM responds more strongly to the imposed differences in  
801 vegetation than RCA4. This explains some of the differences between the climate conditions  
802 simulated by RCA4 and HCLIM, and also means that the choice of vegetation is even more  
803 important in HCLIM. It is unfortunately difficult to assess which model has the most realistic  
804 response. Proxy datasets are not consistent and have large uncertainties, and proxy-based climate  
805 reconstructions, especially quantitative records, are sparse for the 6 ka period. Furthermore, model  
806 performance is dependent on many other factors: such as large-scale circulation, parametrisations  
807 and resolution to name a few. The best way to manage this model uncertainty is to use several  
808 models to try to capture the range of possible climates. It should be noted that the choice of GCM is  
809 also an important contribution to the simulated climate. We were able to use only one GCM in this  
810 study, but we show that the use of another GCM would give different, but still comparable, results.  
811 The importance of the combination of GCM and RCM has been emphasised previously (e.g.

812 Kjellström et al., 2018; Sørland et al., 2018), but has not been acknowledged sufficiently in  
813 downscaling exercises for past climates, even though there are recent studies using several GCMs  
814 or perturbed physics ensembles (Russo et al., 2021; Stadelmeier et al., 2021). The importance of  
815 model and vegetation choice calls for caution when designing palaeo climate experiments. Here we  
816 show that it is essential to have a good, well-motivated description of vegetation to simulate the  
817 same climate with different models in a model ensemble.

818

819 The climate change between 6 ka and PI is not only explained by variations in land cover. The  
820 distinctions are mainly explained by strong differences in solar insolation (e.g. Wanner et al., 2008;  
821 Renssen et al., 2009). This means that all models of quality will simulate similar 6 ka conditions,  
822 largely regardless of land cover. The differences in climate are small compared to other  
823 uncertainties in models and proxies. Nevertheless, the amount of LULCC used in this study (the  
824 difference between potential and reconstructed land cover) is large enough to exert a significant  
825 impact on the simulated climate. Consequently, it is likely that there was already an anthropogenic  
826 impact on European climate at 6 ka. We suggest that LULCC at 6 ka made parts of southern Europe  
827 around 0.5 °C warmer in summer. These relatively strong responses have some important  
828 implications:

829

- 830 i) Anthropogenic land cover changes may have already affected European  
831 temperatures at 6 ka.
- 832 ii) Simulated climate is sensitive to land cover. It is therefore important to use a land  
833 cover reconstruction that is both realistic and consistent with the simulated climate.
- 834 iii) Models respond to changes in land cover in different ways. It is therefore important  
835 to estimate model uncertainty by using model ensembles.



836 iv) Land cover-changes are also important for understanding future climate and should  
837 be included in simulations of the future.

838

839

## 840 **Data availability**

841 RCM data is available via the Bolin Centre Database [https://doi.org/10.17043/strandberg-2022-](https://doi.org/10.17043/strandberg-2022-landclim-ii-1)  
842 [landclim-ii-1](https://doi.org/10.17043/strandberg-2022-landclim-ii-1).

843 DVM produced estimates of 6k land cover are stored in DataGURU (<https://dataguru.lu.se/>).

844

## 845 **Acknowledgements**

846 This study was funded by a research project financed by the Swedish Research Council VR

847 (Vetenskapsrådet) on “Quantification of the bio-geophysical and biogeochemical forcings from  
848 anthropogenic de-forestation on regional Holocene climate in Europe, LandClim II”.

849 EC-Earth, RCA4 and HCLIM simulations and analyses were performed on the Swedish climate

850 computing resource Bi provided by the Swedish National Infrastructure for Computing (SNIC) at

851 the Swedish National Supercomputing Centre (NSC) at Linköping University. Financial support

852 from the Linnaeus University’s Faculty of Health and Life Science is acknowledged for Marie-José

853 Gaillard, Anna-Kari Trondman, and Esther Githumbi. Qiong Zhang acknowledges financial support

854 from the Swedish Research Council VR project 2013-06476 and 2017-04232. Anneli Poska

855 acknowledges support by Estonian Research Council grant PRG323. This is a contribution to the

856 strategic research areas MERGE (Modelling the Regional and Global Earth system), the Bolin

857 Centre for Climate Research, and the PAGES LandCover6k working group that, in turn, received

858 support from the Swiss National Science Foundation, US National Science Foundation, Swiss

859 Academy of Sciences, and Chinese Academy of Sciences.

860

861

862 **References**

863

864 Aitchison, J., 1986. The statistical analysis of compositional data, Chapman & Hall, Ltd, London.

865

866 Arneth, A., F. Denton, F. Agus, A. Elbehri, K. Erb, B. Osman Elasha, M. Rahimi, M. Rounsevell,  
867 A. Spence, R. Valentini, 2019. Framing and Context. In: Climate Change and Land: an IPCC  
868 special report on climate change, desertification, land degradation, sustainable land management,  
869 food security, and greenhouse gas fluxes in terrestrial ecosystems [P.R. Shukla, J. Skea, E. Calvo  
870 Buendia, V. Masson-Delmotte, H.-O. Pörtner, D.C. Roberts, P. Zhai, R. Slade, S. Connors, R. van  
871 Diemen, M. Ferrat, E. Haughey, S. Luz, S. Neogi, M. Pathak, J. Petzold, J. Portugal Pereira, P.  
872 Vyas, E. Huntley, K. Kissick, M. Belkacemi, J. Malley, (eds.)]. In press.

873

874 Augustin, L., Barbante, C., Barnes, P. et al., 2010. Eight glacial cycles from an Antarctic ice  
875 core. *Nature* 429, 623–628. <https://doi.org/10.1038/nature02599>

876

877 Bader, J., Jungclaus, J., Krivova, N., Lorenz, S., Maycock, A., Raddatz, T., Schmidt, H., Toohey,  
878 M., Wu, C.-J., Claussen, M., 2020. Global temperature modes shed light on the Holocene  
879 temperature conundrum, *Nature Communications*, 4726, 11, 1. doi: 10.1038/s41467-020-18478-6

880

881 Bartlein, P. J., Harrison, S. P., Brewer, S., Connor, S., Davis, B. A. S., Gajewski, K., Guiot, J.,  
882 Harrison-Prentice, T. I., Henderson, A., Peyron, O., Prentice, I. C., Scholze, M., Seppä, H.,  
883 Shuman, B., Sugita, S., Thompson, R. S., Vial, A. E., Williams, J. and Wu, H. 2011. Pollen-based  
884 continental climate reconstructions at 6 and 21 ka: A global synthesis, *Clim. Dyn.*, 37(3–4),  
885 775–802. doi:10.1007/s00382-010-0904-1

886

887 Bartlein, P. J., S. P. Harrison, and K. Izumi, 2017. Underlying causes of Eurasian  
888 midcontinental aridity in simulations of mid-Holocene climate, *Geophys. Res. Lett.*, 44, 9020–9028. doi:10.1002/2017GL074476.

889

891 Bazile, E., Marquet, P., Bouteloup, Y., and Bouyssel, F.: The Turbulent Kinetic Energy (TKE)  
892 scheme in the NWP models at Meteo France, in: Workshop on Workshop on Diurnal cycles and the  
893 stable boundary layer, 7–10 November 2011, 127–135, ECMWF, Shinfield Park, Reading,  
894 available at: <https://www.ecmwf.int/node/8006> (last access: 18 March 2020), 2012.

895

896 Bechtold, P., Bazile, E., Guichard, F., Mascart, P., and Richard, E.: A mass-flux convection scheme  
897 for regional and global models, *Q. J. Roy. Meteorol. Soc.*, 127, 869–886, 2001.

898

899 Belušić, D., Fuentes-Franco, R., Strandberg, G. and Jukimenko, A., 2019. Afforestation reduces  
900 cyclone intensity and precipitation extremes over Europe. *Environ. Res. Lett.* 14.  
<https://doi.org/10.1088/1748-9326/ab23b2>

901

902 Belušić, D., de Vries, H., Dobler, A., Landgren, O., Lind, P., Lindstedt, D., Pedersen, R. A.,  
903 Sánchez-Perrino, J. C., Toivonen, E., van Ulft, B., Wang, F., Andrae, U., Batrak, Y., Kjellström, E.,  
904 Lenderink, G., Nikulin, G., Pietikäinen, J.-P., Rodríguez-Camino, E., Samuelsson, P., van  
905 Meijgaard, E., and Wu, M., 2020. HCLIM38: a flexible regional climate model applicable for  
906 different climate zones from coarse to convection-permitting scales, *Geosci. Model Dev.*, 13,  
907 1311–1333, <https://doi.org/10.5194/gmd-13-1311-2020>.

908

909 Bigler, C., Grahn, E., Larocque, I., Jeziorski, A., and Hall, R., 2003. Holocene environmental  
910 change at Lake Njulla (999 m a.s.l.), northern Sweden: a comparison with four small nearby lakes  
911 along an altitudinal gradient, *J. Paleolimnol.*, 29, 13–29. <https://doi.org/10.1023/A:1022850925937>

912

913 Bigler, C., Barnekow, L., Heinrichs, M. L., and Hall, R. I., 2006. Holocene environmental history of  
914 Lake Vuolop Njakajaure (Abisko National Park, northern Sweden) reconstructed using biological  
915 proxy indicators, *Veget. Hist. Archaeobot.*, 15, 309–320. <https://doi.org/10.1007/s00334-006-0054-x>  
916

917 Binney, H.A., Gething, P., Sugita, S., Nield, J., and Edwards, M.E. 2011. Tree line identification  
918 from pollen data: beyond the limit? *Journal of Biogeography*, 38, 1792-1806. DOI: 10.1111/j.1365-  
919 2699.2011.02507.x

920 Bocquet-Appel, J.-P. (2011). "When the World's Population Took Off: The Springboard of the  
921 Neolithic Demographic Transition". *Science*. **333** (6042): 560–561.

922 Boé, J., Somot, S., Corre, L., Nabat, P., 2020. Large discrepancies in summer climate change over  
923 Europe as projected by global and regional climate models: causes and consequences. *Clim*  
924 *Dyn* 54, 2981–3002.. <https://doi.org/10.1007/s00382-020-05153-1>  
925

926 Bonferroni, C. E., 1936. *Teoria statistica delle classi e calcolo delle probabilità*, Pubblicazioni del R  
927 Istituto Superiore di Scienze Economiche e Commerciali di Firenze.

928 Borgmark, A., 2005. Holocene climate variability and periodicities in south-central Sweden  
929 interpreted from peat humification analysis, *Holocene*, 15, 387–395.  
930 <https://doi.org/10.1191/0959683605hl816rp>

931 Bouteloup, Y., Bouyssel, F., and Marquet, P.: Improvements of Lopez’s prognostic large scale  
932 cloud and precipitation scheme, *ALADIN Newsletter*, 28, 66–73, 2005.  
933

934 Boysen, L. R., Brovkin, V., Pongratz, J., Lawrence, D. M., Lawrence, P., Vuichard, N., Peylin, P.,  
935 Liddicoat, S., Hajima, T., Zhang, Y., Rocher, M., Delire, C., Séférian, R., Arora, V. K., Nieradzik,  
936 L., Anthoni, P., Thiery, W., Laguë, M. M., Lawrence, D., and Lo, M.-H., 2020. Global climate  
937 response to idealized deforestation in CMIP6 models, *Biogeosciences*, 17, 5615–5638.  
938 <https://doi.org/10.5194/bg-17-5615-2020>.

939 Braconnot, P., Harrison, S. P., Kageyama, M., Bartlein, P. J., Masson-Delmotte, V., Abe-Ouchi, A.,  
940 Otto-Bliesner, B. and Zhao, Y., 2012. Evaluation of climate models using palaeoclimatic data,  
941 *Nature Climate Change* 2, 417-424. doi:10.1038/nclimate1456

942 Breil, M., Rechid, D., Davin, E. L., de Noblet-Ducoudré, N., Katragkou, E., Cardoso, R. M.,  
943 Hoffmann, P., Jach, L. L., Soares, P. M. M., Sofiadis, G., Strada, S., Strandberg, G., Tölle, M. H.,  
944 Warrach-Sagi, K., 2020. The opposing effects of re/af-forestation on the diurnal temperature cycle  
945 at the surface and in the lowest atmospheric model level in the European summer, *Journal of*  
946 *Climate*, 33,21, 9159-9179. DOI:<https://doi.org/10.1175/JCLI-D-19-0624.1>

947 Brierley, C. M., Zhao, A., Harrison, S. P., Braconnot, P., Williams, C. J. R., Thornalley, D. J. R.,  
948 Shi, X., Peterschmitt, J.-Y., Ohgaito, R., Kaufman, D. S., Kageyama, M., Hargreaves, J. C., Erb, M.  
949 P., Emile-Geay, J., D'Agostino, R., Chandan, D., Carré, M., Bartlein, P. J., Zheng, W., Zhang, Z.,  
950 Zhang, Q., Yang, H., Volodin, E. M., Tomas, R. A., Routson, C., Peltier, W. R., Otto-Bliesner, B.,  
951 Morozova, P. A., McKay, N. P., Lohmann, G., Legrande, A. N., Guo, C., Cao, J., Brady, E., Annan,  
952 J. D., and Abe-Ouchi, A. 2020. Large-scale features and evaluation of the PMIP4-CMIP6  
953 midHolocene simulations, *Clim. Past*, 16, 1847–1872. <https://doi.org/10.5194/cp-16-1847-2020>.

954 Brooks, S., Gelman, A., Jones, G. L., and Meng, X.-L., 2011. *Handbook of Markov chain Monte*  
955 *Carlo*. Boca Raton, FL; CRC Press.  
956

957 Christensen, O.B. and Kjellström, E. Partitioning uncertainty components of mean climate and  
958 climate change in a large ensemble of European regional climate model projections, 2020. *Clim*  
959 *Dyn* 54, 4293–4308. <https://doi.org/10.1007/s00382-020-05229-y>  
960

961 Cuxart, J., Bougeault, P., and Redelsperger, J.-L.: A turbulence scheme allowing for mesoscale and  
962 large-eddy simulations, *Q. J. Roy. Meteorol. Soc.*, 126, 1–30,  
963 <https://doi.org/10.1002/qj.49712656202>, 2000.

964  
965 Davin, E. L., Rechid, D., Breil, M., Cardoso, R. M., Coppola, E., Hoffmann, P., Jach, L. L.,  
966 Katragkou, E., de Noblet-Ducoudré, N., Radtke, K., Raffa, M., Soares, P. M. M., Sofiadis, G.,  
967 Strada, S., Strandberg, G., Tölle, M. H., Warrach-Sagi, K., and Wulfmeyer, V., 2020.  
968 Biogeophysical impacts of forestation in Europe: First results from the LUCAS (Land Use and  
969 Climate Across Scales) regional climate model intercomparison. *Earth Syst. Dyn.*, 11, 183–200.  
970 <https://doi.org/10.5194/esd-11-183-2020>.

971  
972 Dawson, A., Cao, X., Chaput, M., Hopla, E., Li, F., Edwards, M., Fyfe, R., Gajewski, K., Goring, S.  
973 J., Herzschuh, U., Mazier, F., Sugita, S., Williams, J. W., Xu, Q., and Gaillard, M.-J., 2018. A  
974 spatially explicit pollen-based reconstruction of Northern Hemisphere land cover suggests open  
975 land increases of 10 to 100% across large parts of the study area over the period 6 and 0.2 ka BP.  
976 This change may have influenced past climate. *Past Global Changes Magazine*, vol. 26(1), 34-35.  
977 <https://doi.org/10.22498/pages.26.1.34>

978  
979 Diaconu, A.-C., Tóth, M., Lamentowicz, M., Heiri, O., Kuske, E., Tanțău, I., Panait, A.-M., Braun,  
980 M., Feurdean, A., 2017. How warm? How wet? Hydroclimate reconstruction of the past 7500years  
981 in northern Carpathians, Romania, *Palaeogeography, Palaeoclimatology, Palaeoecology*, Volume  
982 482, 2017, Pages 1-12. <https://doi.org/10.1016/j.palaeo.2017.05.007>.

983  
984 Digerfeldt, G., 1998. Reconstruction and regional correlation of Holocene lake-level fluctuations in  
985 Lake Bysjön, South Sweden, *Boreas*, 17, 165–182. [https://doi.org/10.1111/j.1502-](https://doi.org/10.1111/j.1502-3885.1988.tb00544.x)  
986 [3885.1988.tb00544.x](https://doi.org/10.1111/j.1502-3885.1988.tb00544.x)

987  
988 Dosio, A., Turner, A.G., Tamoffo, A.T., Sylla, M.B., Lennard, C., Jones, R.G., Terray, L., Nikulin,  
989 G. and Hewitson, B., 2020. A tale of two futures: contrasting scenarios of future precipitation for  
990 West Africa from an ensemble of regional climate models. *Environ. Res. Lett.* 15, 064007.  
991 <https://doi.org/10.1088/1748-9326/ab7fde>

992  
993 Dufresne, J. L., Foujols, M. a., Denvil, S., Caubel, A., Marti, O., Aumont, O., Balkanski, Y., Bekki,  
994 S., Bellenger, H., Benshila, R., Bony, S., Bopp, L., Braconnot, P., Brockmann, P., Cadule, P.,  
995 Cheruy, F., Codron, F., Cozic, A., Cugnet, D., de Noblet, N., Duvel, J. P., Ethé, C., Fairhead, L.,  
996 Fichefet, T., Flavoni, S., Friedlingstein, P., Grandpeix, J. Y., Guez, L., Guilyardi, E., Hauglustaine,  
997 D., Hourdin, F., Idelkadi, A., Ghattas, J., Joussaume, S., Kageyama, M., Krinner, G., Labetoulle, S.,  
998 Lahellec, A., Lefebvre, M. P., Lefevre, F., Levy, C., Li, Z. X., Lloyd, J., Lott, F., Madec, G.,  
999 Mancip, M., Marchand, M., Masson, S., Meurdesoif, Y., Mignot, J., Musat, I., Parouty, S., Polcher,  
1000 J., Rio, C., Schulz, M., Swingedouw, D., Szopa, S., Talandier, C., Terray, P., Viovy, N., and  
1001 Vuichard, N., 2013. Climate change projections using the IPSL-CM5 Earth System Model: From  
1002 CMIP3 to CMIP5, *Climate Dynamics*, 40, 2123–2165. doi:10.1007/s00382-012-1636-1.

1003  
1004 Fischer, N. and Jungclaus, J. H., 2011. Evolution of the seasonal temperature cycle in a transient  
1005 Holocene simulation: orbital forcing and sea-ice, *Clim. Past*, 7, 1139–1148, doi:10.5194/cp-7-1139-  
1006 2011.

1007  
1008 Flato, G., J. Marotzke, B. Abiodun, P. Braconnot, S.C. Chou, W. Collins, P. Cox, F. Driouech, S.  
1009 Emori, V. Eyring, C. Forest, P. Gleckler, E. Guilyardi, C. Jakob, V. Kattsov, C. Reason and  
1010 Rummukainen, M., 2013. Evaluation of Climate Models. In: *Climate Change 2013: The Physical  
1011 Science Basis. Contribution of Working Group I to the Fifth Assessment Report of the  
1012 Intergovernmental Panel on Climate Change* [Stocker, T.F., D. Qin, G.-K. Plattner, M. Tignor, S.K.

1013 Allen, J. Boschung, A. Nauels, Y. Xia, V. Bex and P.M. Midgley (eds.)]. Cambridge University  
1014 Press, Cambridge, United Kingdom and New York, NY, USA.

1015

1016 Fouquart, Y. and Bonnel, B.: Computations of solar heating of the earth's atmosphere: A new  
1017 parameterization, *Beitrage zur Physik der Atmosphere*, 53, 35–62, 1980.

1018

1019 Gaillard, M.-J., Sugita, S., Mazier, F., Trondman, A.-K., Broström, A., Hickler, T., Kaplan, J. O.,  
1020 Kjellström, E., Kokfelt, U., Kuneš, P., Lemmen, C., Miller, P., Olofsson, J., Poska, A., Rundgren,  
1021 M., Smith, B., Strandberg, G., Fyfe, R., Nielsen, A. B., Alenius, T., Balakauskas, L., Barnekow, L.,  
1022 Birks, H. J. B., Bjune, A., Björkman, L., Giesecke, T., Hjelle, K., Kalnina, L., Kangur, M., van der  
1023 Knaap, W. O., Koff, T., Lagerås, P., Latalowa, M., Leydet, M., Lechterbeck, J., Lindbladh, M.,  
1024 Odgaard, B., Peglar, S., Segerström, U., von Stedingk, H., and Seppä, H., 2010: Holocene land  
1025 cover reconstructions for studies on land cover-climate feedbacks, *Clim. Past*, 6, 483–499.  
1026 doi:10.5194/cp-6-483-2010.

1027

1028 Gałka, M. and Apolinarska, K., 2014. Climate change, vegetation development, and lake level  
1029 fluctuations in Lake Purwin (NE Poland) during the last 8600 cal. BP based on a high-resolution  
1030 plant macrofossil record and stable isotope data ( $\delta^{13}\text{C}$  and  $\delta^{18}\text{O}$ ). *Quaternary International* 328-  
1031 329, 213-225. <https://doi.org/10.1016/j.quaint.2013.12.030>.

1032

1033 Gao, Y., T. Markkanen, L. Backman, H. M. Henttonen, J.-P. Pietikäinen, H. M. Mäkelä, and  
1034 Laaksonen, A., 2014. Biogeophysical impacts of peatland forestation on regional climate changes  
1035 in Finland. *Biogeosciences*, 11, 7251–7267. <https://doi.org/10.5194/bg-11-7251-2014>.

1036

1037 Garreta, V., Miller, P. A., Guiot, J., Hély, C., Brewer, S., Sykes, M. T., Litt, T., 2010. A method for  
1038 climate and vegetation reconstruction through the inversion of a dynamic vegetation model. *Climate*  
1039 *Dynamics* 35: 371-389. <https://doi.org/10.1007/s00382-009-0629-1>

1040

1041 Gilgen, A., Wilkenskjeld, S., Kaplan, J. O., Kühn, T. and Lohmann, U., 2019. Effects of land use  
1042 and anthropogenic aerosol emissions in the Roman Empire. *Clim. Past*, 15, 1885–1911.  
1043 <https://doi.org/10.5194/cp-15-1885-2019>

1044

1045 Giorgi F., 2019. Thirty years of regional climate modeling: Where are we and where are we going  
1046 next? *Journal of Geophysical Research: Atmospheres* 124: 5696-5723.  
1047 <https://doi.org/10.1029/2018JD030094>

1048

1049 Githumbi, E., Fyfe, R., Gaillard, M.-J., Trondman, A.-K., Mazier, F., Nielsen, A.-B., Poska, A.,  
1050 Sugita, S., Theuerkauf, M., Woodbridge, J., Azuara, J., Feurdean, A., Grindean, R., Lebreton, V.,  
1051 Marquer, L., Nebout-Combourieu, N., Stancikaite, M., Tanțău, I., Tonkov, S., Shumilovskikh, L.,  
1052 and the LandClimII Data Contributors, 2021. European pollen-based REVEALS land-cover  
1053 reconstructions for the Holocene: methodology, mapping and potentials, *Earth Syst. Sci. Data*  
1054 *Discuss.* [preprint], <https://doi.org/10.5194/essd-2021-269>, in review.

1055

1056 Griscom, B. W., Adams, J., Ellis, P. W., Houghton, R. A., Lomax, G., Miteva, D. A., Schlesinger,  
1057 W. H., Shoch, D., Siikamäki, J. V., Smith, P., Woodbury, P., Zganjar, C., Blackman, A., Richard J.  
1058 C., Conant, T., Delgado, C., Elias, P., Gopalakrishna, T., Hamsik, M. R., Herreso, M., Kiesecker,  
1059 J., Landis, E., Laestadius, L., Leavitt, S. M., Minnemeyer, S., Polasky, S., Potapov, P., Putz, F. E.,  
1060 Sanderman, J., Silvius, M., Wollenberg, E., Fargione, J., 2017. Natural climate solutions,  
1061 *PNAS*, 114 (44) 11645-11650; DOI: 10.1073/pnas.1710465114

1062

1063 Grudd, H., 2002. A 7400-year tree-ring chronology in northern Swedish Lapland: natural climatic  
1064 variability expressed on annual to millennial timescales, *Holocene*, 12, 657–665.

1065 <https://doi.org/10.1191/0959683602hl578rp>.  
1066  
1067 Hammarlund, D., Björck, S., Buchardt, B., Israelson, C., and Thomsen, C. T., 2003. Rapid  
1068 hydrological changes during the Holocene revealed by stable isotope records of lacustrine  
1069 carbonates from Lake Igelsjön, southern Sweden, *Quaternary Sci. Rev.*, 22, 353–370.  
1070 [https://doi.org/10.1016/S0277-3791\(02\)00091-4](https://doi.org/10.1016/S0277-3791(02)00091-4)  
1071  
1072 Hammarlund, D., Velle, G., Wolfe, B. B., Edwards, T. W. D., Barnekow, L., Bergman, J.,  
1073 Holmgren, S., Lamme, S., Snowball, I., Wohlfarth, B., and Possnert, G., 2004. Palaeolimnological  
1074 responses to Holocene forest retreat in the Scandes Mountains, west-central Sweden, *Holocene*, 14,  
1075 862–876. <https://doi.org/10.1191/0959683604hl756rp>  
1076  
1077 Harrison, S., Bartlein, P., Izumi, K., Li, G., Annan, J., Hargreaves, J., Braconnot, P. and Kageyama,  
1078 M., 2015. Evaluation of CMIP5 palaeo-simulations to improve climate projections. *Nature Clim*  
1079 *Change* 5, 735–743. <https://doi.org/10.1038/nclimate2649>  
1080  
1081 Harrison, S. P., Bartlein, P. J., Brovkin, V., Houweling, S., Kloster, S. and Prentice, I. C., 2018. The  
1082 biomass burning contribution to climate-carbon cycle feedback. *Earth System Dynamics*, 9. pp.  
1083 663-677. doi: <https://doi.org/10.5194/esd-9-663-2018>  
1084  
1085 Harrison, S. P., Gaillard, M. J., Stocker, B. D., Vander Linden, M., Klein Goldewijk, K., Boles, O.,  
1086 Braconnot, P., Dawson, A., Fluet-Chouinard, E., Kaplan, J. O., Kastner, T., Pausata, F. S. R.,  
1087 Robinson, E., Whitehouse, N. J., Madella, M. and Morrison, K. D., 2020. Development and testing  
1088 of scenarios for implementing Holocene LULC in earth system model experiments. *Geoscientific*  
1089 *Model Development Discussions*, 13 (2). pp. 805-824. ISSN 1991-962X doi:  
1090 <https://doi.org/10.5194/gmd-13-805-2020>  
1091  
1092 Hazeleger, W., Severijns, C., Semmler, T., Ștefănescu, S., Yang, S., Wang, X., Wyser, K., Dutra,  
1093 E., Baldasano, J. M., Bintanja, R., Bougeault, P., Caballero, R., Ekman, A. M. L., Christensen, J.  
1094 H., van den Hurk, B., Jimenez, P., Jones, C., Kållberg, P., Koenigk, T., McGrath, R., Miranda, P.,  
1095 van Noije, T., Palmer, T., Parodi, J. A., Schmith, T., Selten, F., Storelvmo, T., Sterl, A., Tapamo,  
1096 H., Vancoppenolle, M., Viterbo, P. and Willén, U., 2010. EC-Earth - A Seamless Earth-System  
1097 Prediction Approach in Action *BAMS*, 91, 10, 1357–1364.  
1098 <https://doi.org/10.1175/2010BAMS2877.1>  
1099  
1100 He, F., Vavrus S. J., Kutzbach, J. E., Ruddiman, W., F., Kaplan, J. O. and Krumhardt, K. M., 2014.  
1101 Simulating global and local surface temperature changes due to Holocene anthropogenic land cover  
1102 change, *Geophys. Res. Lett.*, 41, 623–631. doi:10.1002/2013GL058085.  
1103  
1104 Heinrichs, M., Barnekow, L. and Rosenberg, S. A., 2006. comparison of chironomid biostratigraphy  
1105 from Lake Vuolep Njakajaure with vegetation, lake-level, and climate changes in Abisko National  
1106 Park, Sweden. *J Paleolimnol* 36, 119–131. <https://doi.org/10.1007/s10933-006-0010-x>  
1107  
1108 Heinrichs, M. L., Peglar, S. M., Bigler, C. & Birks, H. J. B. 2005. A multi-proxy palaeoecological  
1109 study of Alanen Laanijärvi, a boreal-forest lake in Swedish Lapland. *Boreas*, Vol. 34, pp. 192–206.  
1110 <https://doi.org/10.1111/j.1502-3885.2005.tb01015.x>  
1111  
1112 Heiri, O. and Lotter, A.F., 2005. Holocene and Lateglacial summer temperature reconstruction in  
1113 the Swiss Alps based on fossil assemblages of aquatic organisms: a review. *Boreas* 34, 506-516.  
1114 <https://doi.org/10.1080/03009480500231229>  
1115

1116 Helama, S., Lindholm, M., Timonen, M., Meriläinen, J., and Eronen, M., 2002. The supra-long  
1117 Scots pine tree-ring record for Finnish Lapland. Part 2: Interannual to centennial variability in  
1118 summer temperatures for 7500 years, *The Holocene*, 12, 681–687.  
1119 <https://doi.org/10.1191/0959683602hl581rp>  
1120

1121 Hickler, T., Vohland, K., Feehan, J., Miller, P. A., Smith, B., Costa, L., Giesecke, T., Fronzek, S.,  
1122 Carter, T. R., Cramer, W., Kühn, I. and Sykes, M. T., 2012: Projecting the future distribution of  
1123 European potential natural vegetation zones with a generalized, tree species-based dynamic  
1124 vegetation model. *Global Ecology & Biogeography* 21: 50-63.  
1125 <https://doi.org/10.1111/j.1466-8238.2010.00613.x>  
1126

1127 Hughes, P. D. M., Barber, K. E., Langdon, P. G., and Mauquoy, D., 2000. Mire-development  
1128 pathways and palaeoclimatic records from a full Holocene peat archive at Walton Moss, Cumbria,  
1129 England, *Holocene*, 10, 465–479. <https://doi.org/10.1191/095968300675142023>  
1130

1131 Iacono, M. J., Delamere, J. S., Mlawer, E. J., Shephard, M. W., Clough, S. A., and Collins, W. D.:  
1132 Radiative forcing by longlived greenhouse gases: Calculations with the AER radiative transfer  
1133 models, *J. Geophys. Res.-Atmos.*, 113, D13103, <https://doi.org/10.1029/2008JD009944>, 2008.  
1134

1135 Ikonen, L., 1993. Holocene development and peat growth of the raised bog Pesänsuo in  
1136 southwestern Finland, *Bulletin*, Vol. 370, Geological Survey of Finland, Espoo, 1993.  
1137

1138 IPCC, 2018. Summary for Policymakers. In: *Global Warming of 1.5°C. An IPCC Special Report on*  
1139 *the impacts of global warming of 1.5°C above pre-industrial levels and related global greenhouse*  
1140 *gas emission pathways, in the context of strengthening the global response to the threat of climate*  
1141 *change, sustainable development, and efforts to eradicate poverty [Masson-Delmotte, V., P. Zhai,*  
1142 *H.-O. Pörtner, D. Roberts, J. Skea, P.R. Shukla, A. Pirani, W. Moufouma-Okia, C. Péan, R.*  
1143 *Pidcock, S. Connors, J.B.R. Matthews, Y. Chen, X. Zhou, M.I. Gomis, E. Lonnoy, T. Maycock, M.*  
1144 *Tignor, and T. Waterfield (eds.)]. In Press.*  
1145

1146 Jacob, D., Petersen, J., Eggert, B., Alias, A., Christensen, O.B., Bouwer, L.M., Braun, A., Colette,  
1147 A., Déqué, M., Georgievski, G., Georgopoulou, E., Gobiet, A., Menut, L., Nikulin, G., Haensler,  
1148 A., Hempelmann, N., Jones, C., Keuler, K., Kovats, S., Kröner, N., Kotlarski, S., Kriegsmann, A.,  
1149 Martin, E., van Meijgaard, E., Moseley, C., Pfeifer, S., Preuschmann, S., Radermacher, C., Radtke,  
1150 K., Rechid, D., Rounsevell, M., Samuelsson, P., Somot, S., Soussana, J.-F., Teichmann, C.,  
1151 Valentini, R., Vautard, R., Weber, B., Yiou, P., 2019. EURO-CORDEX: New high-resolution  
1152 climate change projections for European impact research, *Regional Environmental Change*, 14, 2,  
1153 pp. 563-578. DOI 10.1007/s10113-013-0499-2

1154 Jerez, S., López-Romero, J.M., Turco, M. et al. Impact of evolving greenhouse gas forcing on the  
1155 warming signal in regional climate model experiments. *Nat Commun* 9, 1304 (2018).  
1156 <https://doi.org/10.1038/s41467-018-03527-y>  
1157

1158 Jia, G., E. Shevliakova, P. Artaxo, N. De Noblet-Ducoudré, R. Houghton, J. House, K. Kitajima, C.  
1159 Lennard, A. Popp, A. Sirin, R. Sukumar, L. Verchot, 2019. Land–climate interactions. In: *Climate*  
1160 *Change and Land: an IPCC special report on climate change, desertification, land degradation,*  
1161 *sustainable land management, food security, and greenhouse gas fluxes in terrestrial ecosystems*  
1162 *[P.R. Shukla, J. Skea, E. Calvo Buendia, V. Masson-Delmotte, H.-O. Pörtner, D.C. Roberts, P.*  
1163 *Zhai, R. Slade, S. Connors, R. van Diemen, M. Ferrat, E. Haughey, S. Luz, S. Neogi, M. Pathak, J.*  
1164 *Petzold, J. Portugal Pereira, P. Vyas, E. Huntley, K. Kissick, M, Belkacemi, J. Malley, (eds.)]. In*  
1165 *press*  
1166

1167 Kageyama, M., Braconnot, P., Harrison, S. P., Haywood, A. M., Jungclaus, J. H., Otto-Bliesner, B.  
1168 L., Peterschmitt, J.-Y., AbeOuchi, A., Albani, S., Bartlein, P. J., Brierley, C., Crucifix, M., Dolan,  
1169 A., Fernandez-Donado, L., Fischer, H., Hopcroft, P. O., Ivanovic, R. F., Lambert, F., Lunt, D. J.,  
1170 Mahowald, N. M., Peltier, W. R., Phipps, S. J., Roche, D. M., Schmidt, G. A., Tarasov, L., Valdes,  
1171 P. J., Zhang, Q., and Zhou, T., 2018. The PMIP4 contribution to CMIP6 – Part 1: Overview and  
1172 overarching analysis plan, *Geosci. Model Dev.*, 11, 1033–1057. [https://doi.org/10.5194/gmd-11-](https://doi.org/10.5194/gmd-11-1033-2018)  
1173 1033-2018.

1174

1175 Kaplan, J., Krumhardt, K., and Zimmermann, N., 2009. The prehistoric and preindustrial  
1176 deforestation of Europe, *Quaternary Sci. Rev.*, 28, 3016–3034.  
1177 <https://doi.org/10.1016/j.quascirev.2009.09.028>

1178

1179 Kaplan, J. O., Krumhardt, K. M., Ellis, E. C., Ruddiman, W. F., Lemmen, C. and Goldewijk, K. K.,  
1180 2010. Holocene carbon emissions as a result of anthropogenic land cover change, *The Holocene*  
1181 1–17. DOI: 10.1177/0959683610386983.

1182

1183 Kaplan, J. O., Krumhardt, K. M., 2011. The KK10 Anthropogenic Land Cover Change scenario for  
1184 the preindustrial Holocene, link to data in NetCDF format. PANGAEA.  
1185 <https://doi.org/10.1594/PANGAEA.871369>

1186

1187 Kaplan, J.O., Krumhardt, K.M., Gaillard, M.-J., Sugita, S., Trondman, A.-K., Fyfe, R., Marquer, L.,  
1188 Mazier, F., Nielsen, A.B, 2017. Constraining the Deforestation History of Europe: Evaluation of  
1189 Historical Land Use Scenarios with Pollen-Based Land Cover Reconstructions. *Land*, 6, 91.  
1190 <https://doi.org/10.3390/land6040091>

1191

1192 Kjellström, E., Brandefelt, J., Näslund, J.-O., Smith, B., Strandberg, G., Voelker, A. H. L. and  
1193 Wohlfarth, B., 2010. Simulated climate conditions in Europe during the Marine Isotope Stage 3  
1194 stadial. *Boreas*. 10.1111/j.1502-3885.2010.00143.x. ISSN 0300-9483.

1195

1196 Kjellström, E., Barring, L., Nikulin, G., Nilsson, C., Persson, N., Strandberg, G, 2016. Production  
1197 and use of regional climate model projections – A Swedish perspective on building climate  
1198 services, *Clim. Serv.* 2-3, 15-29. <http://dx.doi.org/10.1016/j.cliser.2016.06.004>.

1199

1200 Kjellström, E., Nikulin, G., Strandberg, G., Christensen, O. B., Jacob, D., Keuler, K., Lenderink,  
1201 G., van Meijgaard, E., Schär, C., Somot, S., Sørland, S. L., Teichmann, C., and Vautard, R., 2018.  
1202 European climate change at global mean temperature increases of 1.5 and 2 °C above pre-industrial  
1203 conditions as simulated by the EURO-CORDEX regional climate models, *Earth Syst. Dynam.*, 9,  
1204 459–478. <https://doi.org/10.5194/esd-9-459-2018>.

1205

1206 Klein Goldewijk, K., Beusen, A., de Vos, M., and van Drecht, G., 2011. The HYDE 3.1 spatially  
1207 explicit database of human induced land use change over the past 12,000 years, *Global Ecol.*  
1208 *Biogeogr.*, 20, 73–86. <https://doi.org/10.1111/j.1466-8238.2010.00587.x>

1209

1210 Korhola, A., Weckström, J., Holmström, L., and Erästö, P., 2000. A quantitative Holocene climatic  
1211 record from diatoms in northern Fennoscandia, *Quaternary Res.*, 54, 284–294.  
1212 <https://doi.org/10.1006/qres.2000.2153>

1213

1214 Laroque, I. and Hall, R. I., 2004. Holocene temperature estimates and chironomid community  
1215 composition in the Abisko valley, northern Sweden, *Quaternary Sci. Rev.*, 23, 2453–2465.  
1216 <https://doi.org/10.1016/j.quascirev.2004.04.006>



- 1217 Larocque-Tobler, I., Heiri, O., Wehrli, M., 2010. Late Glacial and Holocene temperature changes at  
1218 Egelsee, Switzerland, reconstructed using subfossil chironomids. *Journal of Paleolimnology* 43,  
1219 649-666. <https://doi.org/10.1007/s10933-009-9358-z>  
1220
- 1221 Li, L., Pengfei Lin, P., Yu, Y., Wang, B., Zhou, T., Liu, L., Liu, J., Bao, Q., Xu, S., Huang, W.,  
1222 Xia, K., Pu, Y., Dong, L., Shen, S., Liu, Y., Hu, N., Liu, M., Sun, W., Shi, X., Zheng, W., Wu, B.,  
1223 Song, M., Liu, H., Zhang, X., Wu, G., Xue, W., Huang, X., Yang, G., Song Z. and Qiao, F. 2013.  
1224 The flexible global ocean–atmosphere–land system model, Grid-point Version 2: FGOALS-g2.  
1225 *Adv. Atmos. Sci.*, 30, 543–560 (19). <https://doi.org/10.1007/s00376-012-2140-6>  
1226
- 1227 Lind, P., Belušić, D., Christensen, O.B., Dobler, A., Kjellström, E., Landgren, O., Lindstedt, D.,  
1228 Matte, D., Pedersen, R.A., Toivonen, E. and Wang, F., 2020. Benefits and added value of  
1229 convection-permitting climate modeling over Fenno-Scandinavia. *Clim. Dyn.* DOI:  
1230 10.1007/s00382-020-05359-3.  
1231
- 1232 Lindgren, F., Rue, H., and Lindström, J., 2011. An explicit link between Gaussian fields and  
1233 Gaussian Markov random fields: the stochastic partial differential equation approach. *Journal of the*  
1234 *Royal Statistical Society, Series B: Statistical Methodology*, 73(4), 423–498.  
1235 <https://doi.org/10.1111/j.1467-9868.2011.00777.x>  
1236
- 1237 Liu, Z., Zhu, J., Rosenthal, Y. Zhang, X., Otto-Bliesner, B. L., Timmermann, A., Smith, R. S.,  
1238 Lohmann, G., Zheng, W. and Elison, T., O., 2014. The Holocene temperature conundrum,  
1239 *Proceedings of the National Academy of Sciences*, E3501-E3505, 111, 34.  
1240 10.1073/pnas.1407229111  
1241
- 1242 Lopez, P.: Implementation and validation of a new prognostic large-scale cloud and precipitation  
1243 scheme for climate and dataassimilation purposes, *Q. J. Roy. Meteorol. Soc.*, 128, 229–257,  
1244 <https://doi.org/10.1256/00359000260498879>, 2002.  
1245
- 1246 Ludwig, P., Shao, Y., Kehl, M. and Weniger G.-C., 2018. The Last Glacial Maximum and Heinrich  
1247 event I on the Iberian Peninsula: A regional climate modelling study for understanding human  
1248 settlement patterns, *Global and Planetary Change*, 170, 34-47,  
1249 <https://doi.org/10.1016/j.gloplacha.2018.08.006>  
1250
- 1251 Ludwig, P., Gómez-Navarro, J. J., Pinto, J. G., Raible, C. C., Wagner, S., and Zorita, E., 2019  
1252 Perspectives of regional paleoclimate modeling, *Ann. NY. Acad. Sci.*, 1436, 54-  
1253 69, <https://doi.org/10.1111/nyas.13865>.  
1254
- 1255 Luoto P. T., Kultti S., Nevalainen L., Sarmaja-Korjonen K., 2010. Temperature and effective  
1256 moisture variability in southern Finland during the Holocene quantified with midge-based  
1257 calibration models. *J. Quaternary Sci.*, Vol. 25 pp. 1317–1326. ISSN 0267-8179.
- 1258 Lu, Z., Miller, P. A., Zhang, Q., Zhang, Q., Wårlind, D., Nieradzik, L., Sjolte, J., and Smith, B.:  
1259 Dynamic Vegetation Simulations of the Mid-Holocene Green Sahara, *Geophysical Research*  
1260 *Letters*, 45, 8294-8303, <https://doi.org/10.1029/2018GL079195>, 2018.
- 1261 Magny, M., 2004. Holocene climate variability as reflected by mid-European lake-level fluctuations  
1262 and its probable impact on pre-historic human settlements, *Quaternary Int.*, 113, 65–79.  
1263 [https://doi.org/10.1016/S1040-6182\(03\)00080-6](https://doi.org/10.1016/S1040-6182(03)00080-6)  
1264
- 1265 Marcott, S. A., Shakun, J. D., Clark, P. U. and Mix, A. C., 2013. A reconstruction of

- 1266 regional and global temperature for the past 11,300 years. *Science* 339, 1198–1201. DOI:  
 1267 10.1126/science.1228026.  
 1268
- 1269 Masson, V., Le Moigne, P., Martin, E., Faroux, S., Alias, A., Alkama, R., Belamari, S., Barbu, A.,  
 1270 Boone, A., Bouyssel, F., Brousseau, P., Brun, E., Calvet, J.-C., Carrer, D., Decharme, B., Delire, C.,  
 1271 Donier, S., Essaouini, K., Gibelin, A.-L., Giordani, H., Habets, F., Jidane, M., Kerdraon, G.,  
 1272 Kourzeneva, E., Lafaysse, M., Lafont, S., Lebeaupin Brossier, C., Lemonsu, A., Mahfouf, J.-F.,  
 1273 Marguinaud, P., Mokhtari, M., Morin, S., Pigeon, G., Salgado, R., Seity, Y., Taillefer, F., Tanguy,  
 1274 G., Tulet, P., Vincendon, B., Vionnet, V., and Voldoire, A.: The SURFEXv7.2 land and ocean  
 1275 surface platform for coupled or offline simulation of earth surface variables and fluxes, *Geosci.*  
 1276 *Model Dev.*, 6, 929–960, <https://doi.org/10.5194/gmd-6-929-2013>, 2013.  
 1277  
 1278
- 1279 Mauri, A., Davis, B. A. S., Collins, P. M., and Kaplan, J. O., 2014. The influence of atmospheric  
 1280 circulation on the mid-Holocene climate of Europe: a data–model comparison, *Clim. Past*, 10,  
 1281 1925–1938, <https://doi.org/10.5194/cp-10-1925-2014>.  
 1282
- 1283 Mazier, F., Gaillard, M.-J., Kuneš, P., Sugita, S., Trondman, A.-K., Broström, A., 2012. Testing the  
 1284 effect of site selection and parameter setting on REVEALS-model estimates of plant abundance  
 1285 using the Czech Quaternary Palynological Database. *Rev. Palaeobot. and Palynology*, 187, 38-49.  
 1286 <https://doi.org/10.1016/j.revpalbo.2012.07.017>  
 1287
- 1288 Miller, P. A., Giesecke, T., Hickler, T., Bradshaw, R. H. W., Smith, B., Seppä, H., Valdes, P. J.,  
 1289 Sykes M. T., 2008. Exploring climatic and biotic controls on Holocene vegetation change in  
 1290 Fennoscandia, *J. Ecol.* 96:247-259; doi: 10.1111/j.1365-2745.2007.01342.x  
 1291
- 1292 Mlawer, E. J., Taubman, S. J., Brown, P. D., Iacono, M. J., and Clough, S. A.: Radiative transfer for  
 1293 inhomogeneous atmospheres: RRTM, a validated correlated-k model for the longwave, *J. Geophys.*  
 1294 *Res.-Atmos.*, 102, 16663–16682, <https://doi.org/10.1029/97JD00237>, 1997.  
 1295
- 1296 Monsi M, and Saeki T., 1953. Über den Lichtfaktor in den Pflanzengesellschaften und seine  
 1297 Bedeutung für die Stoffproduktion. *Japanese Journal of Botany* 14: 22-52.  
 1298
- 1299 Muschitiello, F., Zhang, Q., Sundqvist, H. S., Davies, F. J., and Renssen, H.: Arctic climate  
 1300 response to the termination of the African Humid Period, *Quaternary Science Reviews*, 125, 91-97,  
 1301 2015.
- 1302 Niggeman, S., Mangini, A., Richter, D. K., and Wurth, G., 2003. A paleo-climate record of the last  
 1303 17.600 years from the B7 cave, Sauerland, Germany, *Quaternary Sci. Rev.*, 22, 555–567.  
 1304 [https://doi.org/10.1016/S0277-3791\(02\)00143-9](https://doi.org/10.1016/S0277-3791(02)00143-9)  
 1305
- 1306 Olsen, J., Noe-Nygaard, N., and Wolfe, B. B., 2010. Mid to Late Holocene climate variability and  
 1307 anthropogenic impacts; multi-proxy evidence from lake Bliden, Denmark, *J. Paleolimnol.*, 43,  
 1308 323–343. DOI: 10.1007/s10933-009-9334-7
- 1309 Otto-Bliesner, B. L., Braconnot, P., Harrison, S. P., Lunt, D. J., Abe-Ouchi, A., Albani, S., Bartlein,  
 1310 P. J., Capron, E., Carlson, A. E., Dutton, A., Fischer, H., Goelzer, H., Govin, A., Haywood, A.,  
 1311 Joos, F., LeGrande, A. N., Lipscomb, W. H., Lohmann, G., Mahowald, N., Nehrbass-Ahles, C.,  
 1312 Pausata, F. S. R., Peterschmitt, J. Y., Phipps, S. J., Renssen, H., and Zhang, Q.: The PMIP4  
 1313 contribution to CMIP6 – Part 2: Two interglacials, scientific objective and experimental design for

- 1314 Holocene and Last Interglacial simulations, *Geosci. Model Dev.*, 10, 3979-4003, 10.5194/gmd-10-  
1315 3979-2017, 2017.
- 1316 Pausata, F. S. R., Messori, G., and Zhang, Q.: Impacts of dust reduction on the northward expansion  
1317 of the African monsoon during the Green Sahara period, *Earth and Planetary Science Letters*, 434,  
1318 298-307, <https://doi.org/10.1016/j.epsl.2015.11.049>, 2016.
- 1319 Perşoiu, A., Onac, B. P., Wynn, J. G., Blaauw, M., Ionita, M., and Hansson, M., 2017. Holocene  
1320 winter climate variability in Central and Eastern Europe, *Sci. Rep.*, 7: 1196. DOI:10.1038/s41598-  
1321 017-01397-w.
- 1322  
1323 Peyron, O., Combourieu-Nebout, N., Brayshaw, D., Goring, S., Andrieu-Ponel, V., Desprat, S.,  
1324 Fletcher, W., Gambin, B., Ioakim, C., Joannin, S., Kotthoff, U., Kouli, K., Montade, V., Pross, J.,  
1325 Sadori, L., and Magny, M., 2017. Precipitation changes in the Mediterranean basin during the  
1326 Holocene from terrestrial and marine pollen records: a model–data comparison, *Clim. Past*, 13,  
1327 249–265. <https://doi.org/10.5194/cp-13-249-2017>.
- 1328  
1329 Pirzamanbein, B., Lindström, J., Poska, A., and Gaillard, M.-J., 2018. Modelling Spatial  
1330 Compositional Data: Reconstructions of past land cover and uncertainties. *Spatial Statistics*, Vol.  
1331 24, April 2018, Pages 14-31. <https://doi.org/10.1016/j.spasta.2018.03.005>
- 1332  
1333 Pirzamanbein, B., Poska, A. and Lindström, J., 2020. Bayesian Reconstruction of Past Land Cover  
1334 From Pollen Data: Model Robustness and Sensitivity to Auxiliary Variables, *Earth and Space  
1335 Science*, Vol. 7, 1. <https://doi.org/10.1029/2018EA000547>
- 1336  
1337 Prentice, I.C., Sykes, M.T. and Cramer, W., 1993. A simulation model for the transient effects of  
1338 climate change on forest landscapes. *Ecol. Modelling*, 65: 51-70. [https://doi.org/10.1016/0304-  
1339 3800\(93\)90126-D](https://doi.org/10.1016/0304-3800(93)90126-D).
- 1340  
1341 Rana, A., Nikulin, G., Kjellström, E., Strandberg, G., Kupiainen, M., Hansson, U. and Kolax, M.,  
1342 2020. Contrasting regional and global climate simulations over South Asia. *Climate Dynamics*  
1343 volume 54, 2883–2901. <https://doi.org/10.1007/s00382-020-05146-0>
- 1344  
1345 Renssen, H., Seppä, H., Heiri, O., Roche, D.M., Goosse, H. and Fichetfet, T., 2009. The spatial and  
1346 temporal complexity of the Holocene thermal maximum. *Nat. Geosci.* 2, 411–414.  
1347 <https://doi.org/10.1038/ngeo513>
- 1348  
1349 Ritchie, H., Temperton, C., Simmons, A., Hortal, M., Davies, T., Dent, D., and Hamrud, M., 1995.  
1350 Implementation of the Semi-Lagrangian Method in a HighResolution Version of the ECMWF  
1351 Forecast Model, *Mon. Weather Rev.*, 123, 489–514, [https://doi.org/10.1175/1520-  
1352 0493\(1995\)123<0489:IOTSMLM>2.0.CO;2](https://doi.org/10.1175/1520-0493(1995)123<0489:IOTSMLM>2.0.CO;2).
- 1353  
1354 Robert, A. J., Henderson, J., and Turnbull, C., 1972. An implicit scheme for baroclinic models of  
1355 the atmosphere, *Mon. Weather Rev.*, 100, 329–335.
- 1356  
1357 Roberts, G.O. and Stramer, O., 2002. Langevin Diffusions and Metropolis-Hastings Algorithms.  
1358 *Methodology and Computing in Applied Probability* 4, 337–357.  
1359 <https://doi.org/10.1023/A:1023562417138>.
- 1360

- 1361 Roberts, N., Fyfe, R.M., Woodbridge, J., Gaillard, M.-J., Davis, B.A.S., Kaplan, J.O., Marquer, L.,  
1362 Mazier, F., Nielsen, A.B., Sugita, S., Trondman, A.K. and Leydet, M., 2018. Europe's lost forests: a  
1363 pollenbased synthesis for the last 11,000 years, *Sci. Rep.* 8:716. DOI:10.1038/s41598-017-18646-7.  
1364
- 1365 Rosén, P., Segerström, U., Eriksson, L., Renberg, I., and Birks, H. J. B., 2001. Holocene climatic  
1366 change reconstructed from diatoms, chironomids, pollen and near-infrared spectroscopy at an alpine  
1367 lake (Sjuodjijaure) in northern Sweden, *Holocene*, 11, 551–562.  
1368 <https://doi.org/10.1191/095968301680223503>.  
1369
- 1370 Rotstayn, L. D., Jeffrey, S. J., Collier, M. A., Dravitzki, S.M., Hirst, A. C., Syktus, J. I., and Wong,  
1371 K. K., 2012. Aerosol-and greenhouse gas-induced changes in summer rainfall and circulation in the  
1372 Australasian region: a study using single-forcing climate simulations, *Atmos. Chem. Phys.*, 12,  
1373 6377–6404. <https://doi.org/10.5194/acp-12-6377-2012>.  
1374
- 1375 Ruddiman, W. F., Ellis, E. C., Kaplan, J. O., Fuller, D. Q., 2015. Defining the epoch we live in,  
1376 *Science*, 03, 348, 6230, 38-39. DOI: 10.1126/science.aaa7297  
1377
- 1378 Rummukainen, M., 2016. Added value in regional climate modeling, *WIREs Clim Change* 2016,  
1379 7:145–159. doi: 10.1002/wcc.378.  
1380
- 1381 Russo, E. and Cubasch, U., 2016. Mid-to-late Holocene temperature evolution and atmospheric  
1382 dynamics over Europe in regional model simulations. *Clim. Past*, 12, 1645–1662. doi:10.5194/cp-  
1383 12-1645-2016.  
1384
- 1385 Russo, E., Fallah, B., Ludwig, P., Karremann, M., and Raible, C. C., 2021. The long-standing  
1386 dilemma of European summer temperatures at the Mid-Holocene and other considerations on  
1387 learning from the past for the future using a regional climate model, *Clim. Past Discuss.* [preprint],  
1388 <https://doi.org/10.5194/cp-2021-101>, in review.  
1389
- 1390 Schimanke, S., Meier, H. E. M., Kjellström, E., Strandberg, G., and Hordoir, R., 2012. The climate  
1391 in the Baltic Sea region during the last millennium simulated with a regional climate model, *Clim.*  
1392 *Past*, 8, 1419–1433. doi:10.5194/cp-8-1419-2012.  
1393
- 1394 Schmidt, G. A., Kelley, M., Nazarenko, L., Ruedy, R., Russell, G. L., Aleinov, I., Bauer, M., Bauer,  
1395 S. E., Bhat, M. K., Bleck, R., Canuto, S.V., Chen, Y.-h., Cheng, Y., Clune, T. L., Genio, A. D.,  
1396 Fainchtein, R. D., Faluvegi, G., Hansen, J. E., Healy, R. J., Kiang, N. Y., Koch, D., Lacis, A. a.,  
1397 Legrande, A. N., Lerner, J., Lo, K. K., Matthews, E. E., Menon, S., Miller, R. L., Oinas, V., Oloso,  
1398 A. O., Perlwitz, J. P., Puma, M. J., Putman, W. M., Rund, D., Romanou, A., Sato, M., Shindell, D.  
1399 T., Sun, S., Syed, R. A., Tausnev, N., Tsigaridis, K., Unger, N., Voulgarakis, A., Yao, M.-S., and  
1400 Zhang, J., 2014. Configuration and assessment of the GISS ModelE2 contributions to the CMIP5  
1401 archive, *Journal of Advances in Modeling Earth Systems*, 6, 141–184. doi:10.1002/2013MS000265.  
1402
- 1403 Simmons, A. J., Hoskins, B., and Burridge, D., 1978. Stability of the semiimplicit method of time  
1404 integration, *Mon. Weather Rev.*, 106, 405–412.
- 1405 Sitch, S., Smith, B., Prentice, I. C., Arneth, A., Bondeau, A., Cramer, W., Kaplan J. O., Levis, S.,  
1406 Lucht, W., Sykes, M. T., Thonicke, K., and Vevensky, S., 2003. Evaluation of ecosystem dynamics,  
1407 plant geography and terrestrial carbon cycling in the LPJ dynamic global vegetation model. *Global*  
1408 *Change Biology* 9:161-185. <https://doi.org/10.1046/j.1365-2486.2003.00569.x>
- 1409 Smith, B., Prentice, I. C., and Sykes, M. T., 2001. Representation of vegetation dynamics in the  
1410 modelling of terrestrial ecosystems: comparing two contrasting approaches within European climate

- 1411 space, *Global Ecology and Biogeography* 10:621-637. <https://doi.org/10.1046/j.1466->  
1412 822X.2001.t01-1-00256.x
- 1413 Smith, B., Wårlind, D., Arneth, A., Hickler, T., Leadley, P., Siltberg, J., and Zaehle, S., 2014.  
1414 Implications of incorporating N cycling and N limitations on primary production in an individual-  
1415 based dynamic vegetation model, *Biogeosciences* 11: 2027-2054. <https://doi.org/10.5194/bg-11->  
1416 2027-2014.
- 1417 Smith, P., Davis, S., Creutzig, F. et al. 2016a: Biophysical and economic limits to negative  
1418 CO<sub>2</sub> emissions. *Nature Clim Change* 6, 42–50. <https://doi.org/10.1038/nclimate2870>  
1419
- 1420 Smith, M. C., Singarayer, J. S., Valdes, P. J., Kaplan, J. O., and Branch, N. P. 2016b. The  
1421 biogeophysical climatic impacts of anthropogenic land use change during the Holocene, *Clim. Past*,  
1422 12, 923–941. <https://doi.org/10.5194/cp-12-923-2016>.  
1423
- 1424 Snowball, I. and Sandgren, P., 1996. Lake sediment studies of Holocene glacial activity, northern  
1425 Sweden: contrasts in interpretation, *Holocene*, 6, 367–372.  
1426 <https://doi.org/10.1177/095968369600600312>  
1427
- 1428 Stadelmaier, K. H., Ludwig, P., Bertran, P., Antoine, P., Shi, X., Lohmann, G., and Pinto, J. G.,  
1429 2021. A new perspective on permafrost boundaries in France during the Last Glacial Maximum,  
1430 *Clim. Past*, 17, 2559-2576, <https://doi.org/10.5194/cp-17-2559-2021>.  
1431
- 1432 Stevens, B., Giorgetta, M., Esch, M., Mauritsen, T., Crueger, T., Rast, S., Salzmann, M., Schmidt,  
1433 H., Bader, J., Block, K., Brokopf, R., Fast, I., Kinne, S., Kornblueh, L., Lohmann, U., Pincus, R.,  
1434 Reichler, T., and Roeckner, E., 2013. The atmospheric component of the MPI-M earthsystem  
1435 model: ECHAM6, *Journal of Advances in Modeling Earth Systems*, 5, 1–27.  
1436 doi:10.1002/jame.20015, <http://doi.wiley.com/10.1002/jame.20015>, 2013.  
1437
- 1438 Stocker, B. D., Yu, Z., Massa, C., and Joos, F., 2017. Holocene peatland and ice-core data  
1439 constraints on the timing and magnitude of CO<sub>2</sub> emissions from past land use, *P. Natl. Acad. Sci.*  
1440 *USA*, 114, 1492–1497. <https://doi.org/10.1073/pnas.1613889114>.
- 1441 Strandberg, G. and Kjellström, E., 2019. Climate Impacts from Afforestation and Deforestation in  
1442 Europe. *Earth Interact.*, 23, 1–27. <https://doi.org/10.1175/EI-D-17-0033.1>
- 1443 Strandberg, G. and Lind, P., 2021. The importance of horizontal model resolution on simulated  
1444 precipitation. *Weather Clim. Dynam.*, 2, 181–204. <https://doi.org/10.5194/wcd-2-181-2021>
- 1445 Strandberg, G., Brandefelt, J., Kjellström, E. and Smith, B., 2011. High-resolution regional  
1446 simulation of last glacial maximum climate over Europe. *Tellus*, 63A, 107-125. DOI:  
1447 10.1111/j.1600-0870.2010.00485.x.  
1448
- 1449 Strandberg, G., Kjellström, E., Poska, A., Wagner, S., Gaillard, M.-J., Trondman, A.-K., Mauri, A.,  
1450 Davis, B. A. S., Kaplan, J. O., Birks, H. J. B., Bjune, A. E., Fyfe, R., Giesecke, T., Kalnina, L.,  
1451 Kangur, M., van der Knaap, W. O., Kokfelt, U., Kuneš, P., Latalowa, M., Marquer, L., Mazier, F.,  
1452 Nielsen, A. B., Smith, B., Seppä, H., and Sugita, S., 2014. Regional climate model simulations for  
1453 Europe at 6 and 0.2 k BP: sensitivity to changes in anthropogenic deforestation, *Clim. Past*, 10, 661-  
1454 680. doi:10.5194/cp-10-661-2014.  
1455
- 1456 Strandberg, G., Barring, L., Hansson, U., Jansson, C., Jones, C., Kjellström, E., Kolax, M.,  
1457 Kupiainen, M., Nikulin, G., Samuelsson, P., Ullerstig, A., and Wang, S., 2015. CORDEX scenarios

1458 for Europe from the Rossby Centre regional climate model RCA4. SMHI Meteorology and  
1459 Climatology Rep. 116, 84 pp., Norrköping.  
1460 [https://www.smhi.se/polopoly\\_fs/1.90275!/Menu/general/extGroup/attachmentColHold/mainCol1/f](https://www.smhi.se/polopoly_fs/1.90275!/Menu/general/extGroup/attachmentColHold/mainCol1/file/RMK_116.pdf)  
1461 [ile/RMK\\_116.pdf](https://www.smhi.se/polopoly_fs/1.90275!/Menu/general/extGroup/attachmentColHold/mainCol1/file/RMK_116.pdf).  
1462  
1463 Sugita, S., 2007. Theory of quantitative reconstruction of vegetation I: pollen from large sites  
1464 REVEALS regional vegetation composition. *The Holocene*, 17 (2), 229–241.  
1465 <https://doi.org/10.1177/0959683607075837>  
1466  
1467 Sørland, S. L., Schär, C., Lüthi, D. and Kjellström E., 2018. Bias patterns and climate change  
1468 signals in GCM-RCM model chains, *Environ. Res. Lett.*, 13, 074017. [https://doi.org/10.1088/1748-](https://doi.org/10.1088/1748-9326/aacc7)  
1469 [9326/aacc7](https://doi.org/10.1088/1748-9326/aacc7).  
1470  
1471 Temperton, C., Hortal, M., and Simmons, A., 2001. A two-time-level semi-Lagrangian global  
1472 spectral model, *Q. J. Roy. Meteor. Soc.*, 127, 111–127.  
1473  
1474 Trondman, A.-K., Gaillard, M.-J., Mazier, F., Sugita, S., Fyfe, R. M., Nielsen, A. B., Twiddle, C.,  
1475 Barratt, P., Birks, H. J. B., Bjune, A. E., Björkman, L., Broström, A., Caseldine, C. J., David, R.,  
1476 Dodson, J., Dörfler, W., Fischer, E., van Geel, B., Giesecke, T., Hultberg, T., Kalnina, L., Kangur,  
1477 M., van der Knaap, P. W. O, Koff, T., Kunes, P., Lageras, P., Latalowa, M., Lechterbeck, J.,  
1478 Leroyer, C., Leydet, M., Lindbladh, M., Marquer, L., Mitchell, F. J. G., Odgaard, B., V., Peglar, S.  
1479 M., Persson, T., Poska, A., Rösch, M., Seppä, H., Veski, S., Wick, L., 2015. Pollen-based  
1480 quantitative reconstructions of Holocene regional vegetation cover (plant-functional types and land-  
1481 cover types) in Europe suitable for climate modelling. *Global Change Biology*, 21(2), 676-697.  
1482 <https://doi.org/10.1111/gcb.12737>  
1483  
1484 Trondman, A.-K., Gaillard, M.-J., Sugita, S., Björkman, L., Greisman, A., Hultberg, T., Lagerås, P.,  
1485 Lindbladh, M., Mazier, F., 2016. Are pollen records from small sites appropriate for REVEALS  
1486 model-based quantitative reconstructions of past regional vegetation? An empirical test in southern  
1487 Sweden. *Veget. Hist. Archaeobot.*, 25, 131–151. DOI 10.1007/s00334-015-0536-9  
1488  
1489 UNFCCC, 2010. The Cancun Agreements. United Nations Framework Convention on Climate  
1490 Change <http://unfccc.int/meetings/cancunnov2010/meeting/6266.php> (accessed 1 July 2021)  
1491  
1492 X UNFCCC, 2015. The Paris Agreement. United Nations Framework Convention on Climate  
1493 Change, [http://unfccc.int/paris\\_agreement/items/9485.php](http://unfccc.int/paris_agreement/items/9485.php) (accessed 1 July 2021)  
1494  
1495 Valcke, S., 2013. The OASIS3 coupler: a European climate modelling community software, *Geosci.*  
1496 *Model Dev.*, 6, 373-388. doi:10.5194/gmd-6-373-2013  
1497  
1498 Vancoppenolle, M., Fichet, T., Goosse, H., Bouillon, S., Madec, G. and Maqueda, M.A.M., 2009.  
1499 Simulating the mass balance and salinity of arctic and antarctic sea ice. *Ocean Modelling*, 27,  
1500 33–53. <https://doi.org/10.1016/j.ocemod.2008.10.005>  
1501  
1502 Vautard, R., Kadyrov, N., Iles, C., Boberg, F., Buonomo, E., Bülow, K., Coppola, E., Corre, L.,  
1503 Meijgaard, E., Nogherotto, R., Sandstad, M., Schwingshackl, C., Somot, S., Aalbers, E.,  
1504 Christensen, O. B., Ciarlò, J. M., Demory, M.-E., Giorgi, F., Jacob, D., Jones, R. G., Keuler, K.,  
1505 Kjellström, E., Lenderink, G., Levavasseur, G., Nikulin, G., Sillmann, J., Solidoro, C., Sørland, S.  
1506 L., Steger, C., Teichmann, C., Warrach-Sagi, K., and Wulfmeyer, V., 2020. Evaluation of the large  
1507 EURO-CORDEX regional climate model ensemble, *J. Geophys. Res.-Atmos.*, 125.  
1508 e2019JD032344, <https://doi.org/10.1029/2019JD032344>, 2020.

1509

1510 Velasquez, P., Kaplan, J. O., Messmer, M., Ludwig, P., and Raible, C. C., 2021. The role of land  
1511 cover in the climate of glacial Europe, *Clim. Past*, 17, 1161–1180, [https://doi.org/10.5194/cp-17-](https://doi.org/10.5194/cp-17-1161-2021)  
1512 1161-2021.

1513

1514 Velle, G., Brooks, S. J., Birks, H. J. B., and Willassen, E., 2005. Chironomids as a tool for  
1515 inferring Holocene climate: an assessment based on six sites in southern Scandinavia, *Quaternary*  
1516 *Sci. Rev.*, 24, 1429–1462. <https://doi.org/10.1016/j.quascirev.2004.10.010>

1517

1518 Voldoire, A., Sánchez-Gómez, E., Salas y Méliá, D., Decharme, B., Cassou, C., Sénési, S.,  
1519 Valcke, S., Beau, I., Alias, A., Chevallier, M., Déqué, M., Deshayes, J., Douville, H., Fernandez,  
1520 E., Madec, G., Maisonnave, E., Moine, M-P., Planton, S., Saint-Martin, D., Szopa, S., Tyteca, S.,  
1521 Alkama, R., Belamari, S., Braun, A., Coquart, L., Chauvin, F., 2012. The CNRM-CM5.1 global  
1522 climate model: description and basic evaluation. *Clim Dyn.* 40, 2091–2121. doi:10.1007/s00382-  
1523 011-1259-y.

1524

1525 Walczak, I.W., et al., Reconstructing high-resolution climate using CT scanning of unsectioned  
1526 stalagmites: A case study identifying the mid-Holocene onset of the Mediterranean climate in  
1527 southern Iberia, *Quaternary Science Reviews* (2015),  
1528 <http://dx.doi.org/10.1016/j.quascirev.2015.06.013>

1529

1530 Wanner, H., Beer, J., Bütikofer, J., Crowley, T.J., Cubasch, U., Flückiger, J., Goosse, H., Grosjean,  
1531 M., Joos, F., Kaplan, J.O., Küttel, M., Müller, S.A. Prentice, I.C., Solomina, O., Stocker, T.F.,  
1532 Tarasov, P., Wagner, M. and Widmann, M., 2008. Mid- to late Holocene climate change: An  
1533 overview. *Quat. Sci. Rev.* 27, 1791–1828. <https://doi.org/10.1016/j.quascirev.2008.06.013>.

1534

1535 Watanabe, S., Hajima, T., Sudo, K., Nagashima, T., Takemura, T., Okajima, H., Nozawa, T.,  
1536 Kawase, H., Abe, M., Yokohata, T., Ise, T., Sato, H., Kato, E., Takata, K., Emori, S., and  
1537 Kawamiya, M., 2011. MIROC-ESM 2010: model description and basic results of CMIP5-20c3m  
1538 experiments, *Geosci. Model Dev.*, 4, 845–872. <https://doi.org/10.5194/gmd-4-845-2011>.

1539

1540 Williamson, P., 2016: Scrutinize CO2 removal methods. *Nature*, 530, 153-155,  
1541 <https://doi.org/10.1038/530153a>

1542

1543 Wu, T., Song, L., Li, W., Wang, Z., Zhang, H., Xin, X., Zhang, Y., Zhang, L., Li, J., Wu, F., Liu,  
1544 Y., Zhang, F., Shi, X., Chu, M., Zhang, J., Fang, Y., Wang, F., Lu, Y., Liu, X., Wei, M., Liu, Q.,  
1545 Zhou, W., Dong, M., Zhao, Q., Ji, J., Li, L., and Zhou, M., 2014. An overview of BCCclimate  
1546 system model development and application for climate change studies, *Journal of Meteorological*  
1547 *Research*, 28, 34–56. <https://doi.org/10.1007/s13351-014-3041-7>.

1548

1549 Xu, C., Yan, M., Ning, L., Liu, J., 2020. Summer Westerly Jet in Northern Hemisphere during the  
1550 Mid-Holocene: A Multi-Model Study. *Atmosphere*, 11(11):1193.  
1551 <https://doi.org/10.3390/atmos11111193>

1552

1553 Yukimoto, S., Adachi, Y., Hosaka, M., Sakami, T., Yoshimura, H., Hirabara, M., Tanaka, T. Y.,  
1554 Shindo, E., Tsujino, H., Deushi, M., Mizuta, R., Yabu, S., Obata, A., Nakano, H., Koshiro, T.,  
1555 Ose, T., and Kitoh, A., 2012. A New Global Climate Model of the Meteorological Research

1556 Institute: MRI-CGCM3–Model Description and Basic Performance, *J. Meteorol. Soc. Jpn., Ser. II*,  
1557 90A, 23–64. <https://doi.org/10.2151/jmsj.2012-A02>.

1558

1559 Zhang, Q., Bertell, E., Axelsson, J., Chen, J., Han, Z., de Nooijer, W., Lu, Z., Li, Q., Zhang, Q.,  
1560 Wyser, K., and Yang, S., 2021. Simulating the mid-Holocene, last interglacial and mid-Pliocene  
1561 climate with EC-Earth3-LR, *Geosci. Model Dev.*, 14, 1147–1169. [https://doi.org/10.5194/gmd-14-](https://doi.org/10.5194/gmd-14-1147-2021)  
1562 1147-2021.

1563

1564

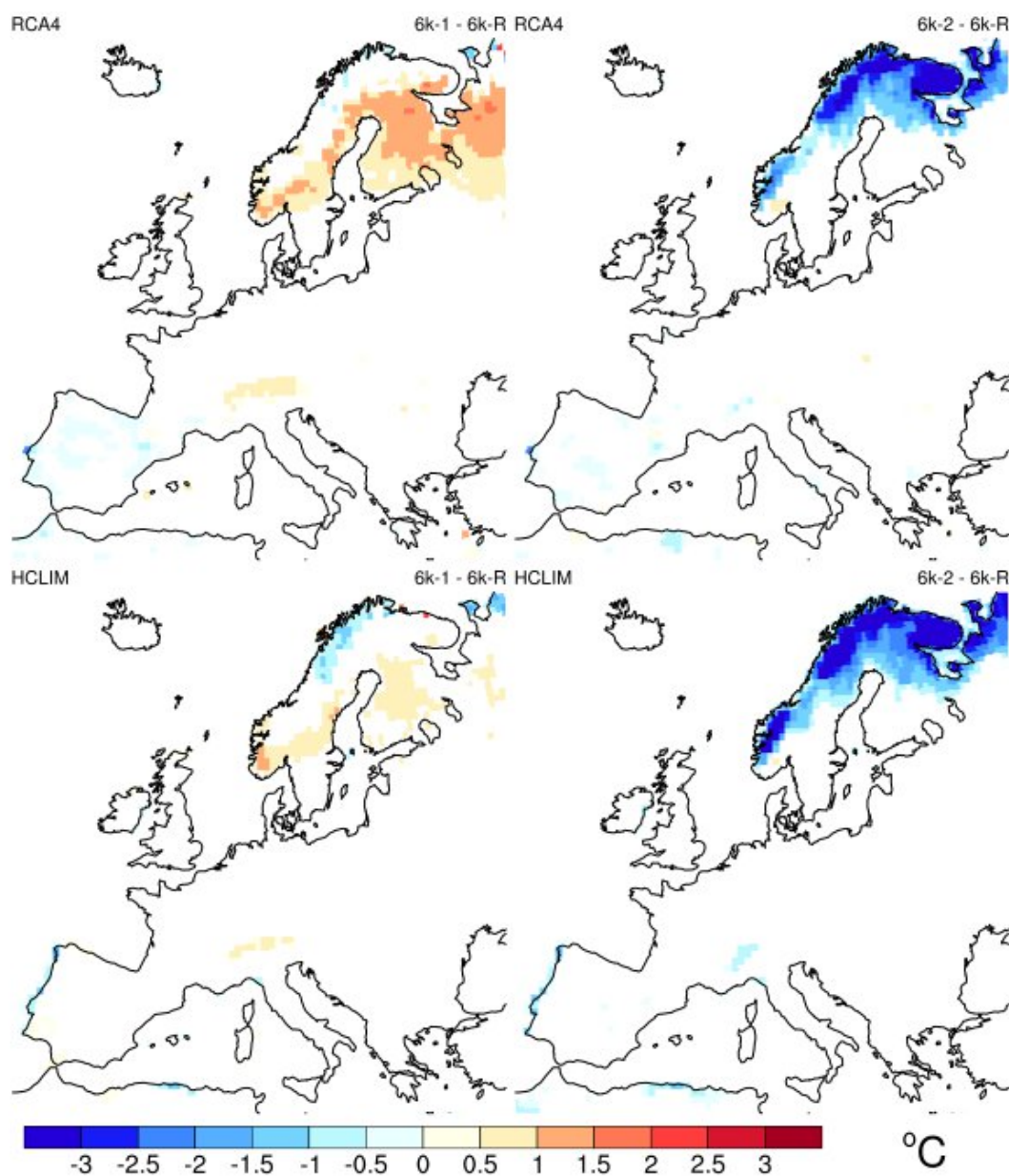
1565

1566



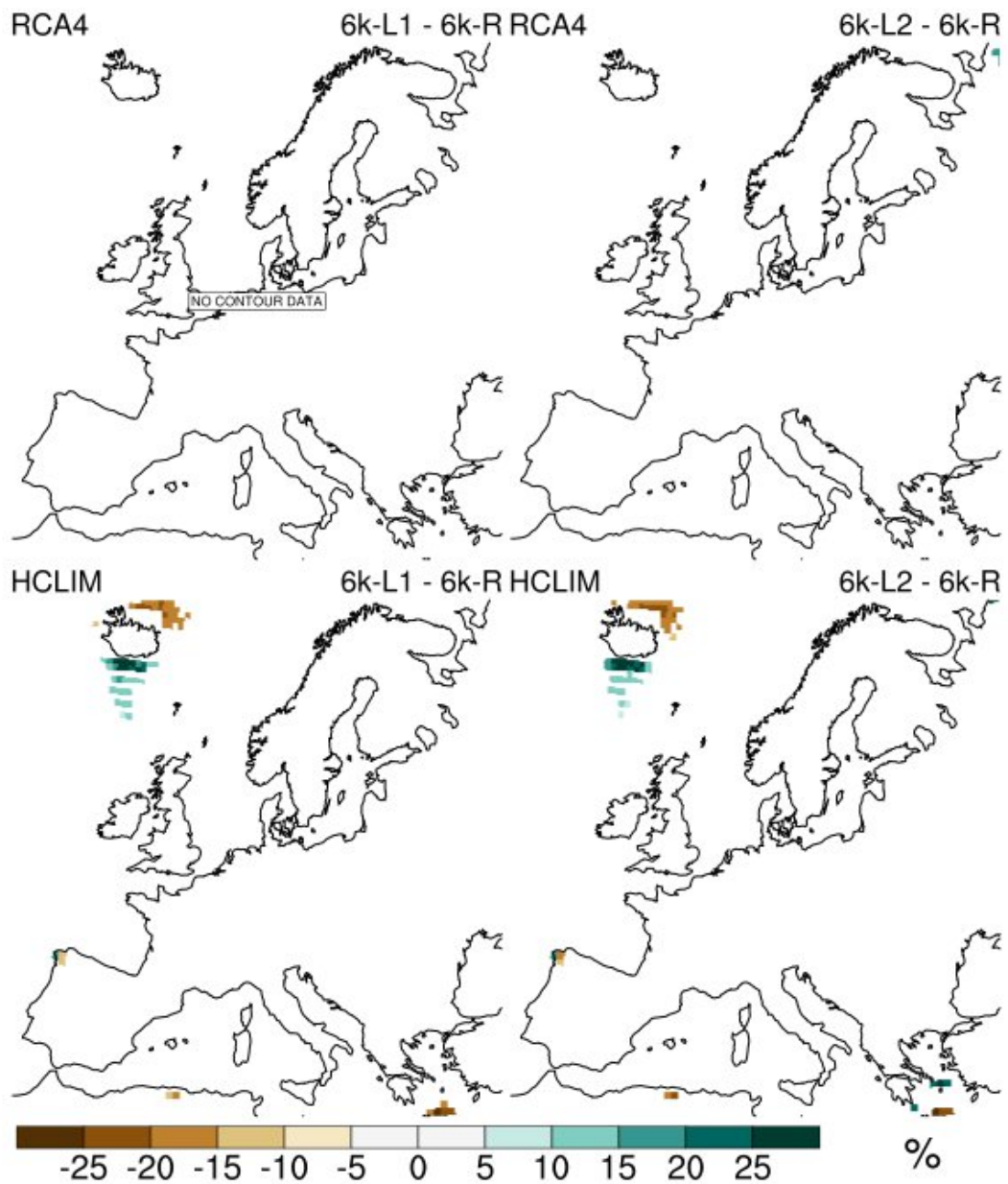
1567  
1568

## Appendix A. Supplementary figures

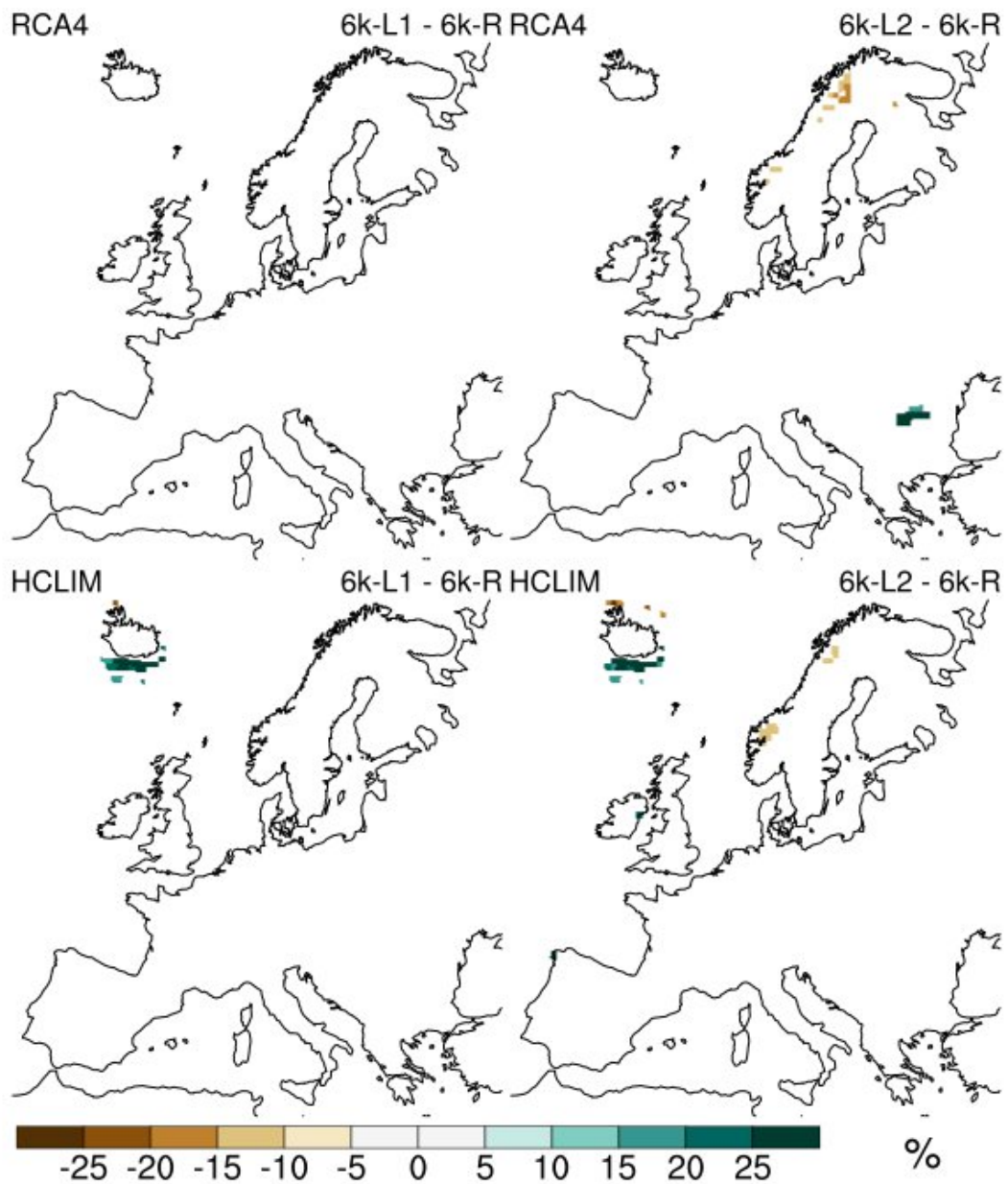


1569  
1570  
1571  
1572  
1573

Fig S1. Difference in surface temperature ( $^{\circ}\text{C}$ ) in spring (March – May) for RCA4 (top row) and HCLIM (bottom row) between 6k-L1 and 6k-R (left column) and 6k-L2 and 6k-R (right column). Only gridboxes that show a significant difference on a 0.05 level are coloured.



1574  
 1575 Fig S2. Difference in precipitation (%) in winter for RCA4 (top row) and HCLIM (bottom row)  
 1576 between 6k-L1 and 6k-R (left column) and 6k-L2 and 6k-R (right column). Only gridboxes that  
 1577 show a significant difference on a 0.05 level are coloured.  
 1578



1579  
 1580 Fig S3. Difference in precipitation (%) in summer for RCA4 (top row) and HCLIM (bottom row)  
 1581 between 6k-L1 and 6k-R (left column) and 6k-L2 and 6k-R (right column). Only gridboxes that  
 1582 show a significant difference on a 0.05 level are coloured.  
 1583